Feature Article

From the glassy state to ordered polymer structures: A microhardness study

A. Flores, F. Ania, F.J. Baltá-Calleja*

Department of Macromolecular Physics, Instituto de Estructura de la Materia, CSIC, Serrano 119, 28006 Madrid, Spain

ABSTRACT

The review covers the understanding of the nanostructure development in glassy and semicrystalline polymers as revealed by indentation hardness methods. The microhardness of polymer glasses is discussed emphasizing the influence of thermal history and physical ageing. The correlation between hardness and glass transition temperature is brought in. Furthermore, the role played by the lamellar morphology in the case of amorphous blends of a block copolymer and a glassy homopolymer is highlighted. A discussion on the influence of filler structure on the microhardness of polymer glasses is introduced. Indentation hardness is presented as a valuable tool to study the kinetics of crystallization from the glassy state. As an example, distinct results on polymer systems under different confinement conditions are shown. The nanostructure–microindentation hardness correlation in the case of semicrystalline polymers and the influence of degree of crystallinity and crystal thickness for various flexible and semirigid polymer systems are recalled. A comprehensive discussion of the creep properties of polymer materials is offered. Concerning deformation mechanisms, experimental results show that for polymers with low degree of crystallinity and T_g below room temperature, a large deviation from the microhardness additivity law is always found. This is due to a different deformation mechanism with respect to that envisaged for polymer materials with T_g above room temperature. The assumption that microhardness approaches zero for amorphous materials above T_g is experimentally confirmed. In the case of an oriented material, it is shown that indentation hardness is capable to detect the gradual appearance of phases of intermediate order. In addition, the study of the creep properties also yields valuable information on the internal degree of order of the oriented system. Finally, an overview of the future perspectives of the application of depth-sensing indentation to the study of polymer materials is offered.

© 2008 Elsevier Ltd. All rights reserved.

1. Introduction

The mechanical behaviour of polymers has been the subject of considerable research in the past [1]. Mechanical properties are of relevance for all the applications of polymers in industry, optics, electronics, photonics, medicine and others [2,3]. Furthermore, the nanostructural and microstructural design of targeted mechanical functional polymer properties is a continuous goal of Materials Science and Engineering [4]. The improvement of the mechanical properties demands a better understanding of the interdependence between molecular structure, morphology and processing methods on the one hand and ultimate mechanical properties on the other, i.e., structure–property correlations [5]. Indentation testing is one of the simplest ways to measure the micromechanical properties of a material, offering the possibility of probing the specimen in its original assembly [6]. One of the advantages of this technique, in comparison to other procedures for mechanical characterization, is

the capability of mapping the surface mechanical properties at a local scale, which is of fundamental importance for inhomogeneous materials. The main applications of indentation hardness to polymer systems have been discussed in detail in preceding reviews [7,8].

Indentation testing is based on the local deformation produced by an indenter upon application of a given load. Conventional microindentation methods are based on the optical measurement of the residual impression produced by the indenter penetrating the material surface. Microhardness, H, is obtained as the ratio of the peak contact load P to the area A of impression ($H = kP/A$). Diamond pyramidal indenters with square (Vickers), rhombus (Knoop) or equilateral triangle (Berkovich) bases are commonly used. For the majority of polymeric materials, the application of loads in the range of 0.05–2 N using a pyramidal indenter gives rise to indentation depths in the micron range. In other words, the surface of the polymer sample is probed "quasi" non-destructively.

During an indentation cycle, plastic deformations are expected to gain importance in the vicinity of the indenter probe (large applied stresses), while elastic behaviour should prevail at low applied stresses, i.e., at locations sufficiently distant from the

* Corresponding author. Tel.: +34 91 5619400; fax: +34 91 5642431.
  E-mail address: imtb421@iem.cfmac.csic.es (F.J. Baltá-Calleja).

hardness impression. The precise stress field for polymers cannot be easily determined because, so far, there is no comprehensive visco-elasto-plastic theory to account for their micromechanical properties. However, valuable attempts have been made in the past to explain the mechanical behaviour of materials that do not exhibit fully plastic behaviour [9,10]. Marsh modelled the elasto-plastic indentation through the expansion of a spherical cavity by an internal pressure [9]. Radial strain contours of hemispherical symmetry around the hardness impression arise from this approach, including the one corresponding to the elastic–plastic boundary. Other different models of elasto-plastic indentation have been proposed to derive the indentation stress field [11–16]. Moreover, numerical–experimental approaches, based on finite element calculations, have been used to calculate the stress distribution under the indenter for specific polymer materials [17–19].

Microhardness can be related to other macroscopic mechanical properties such as yield stress, σ, and elastic modulus, E, both derived from compression testing. For work-hardened metals, Tabor derived a direct proportionality between hardness and compressive yield stress: $H \approx 3\sigma$ [20]. However, it was soon realized that Tabor's relationship only applies to materials that exhibit full plasticity [9,10]. Deviations from this relationship have been reported for a number of metals, glasses and polymers where the elastic strains are non-negligible [9]. Hence, the different expressions describing the correlation of hardness with conventional macroscopic mechanical properties rely on the validity of the above-mentioned elasto-plastic models. In this way, hardness and yield stress no longer hold direct proportionality but their relationship depends on the specific material properties, such as Poisson's ratio and elastic modulus [9,11–13]. It has been shown that these elasto-plastic models not only satisfactorily explain an H/σ ratio of ≈ 2 for a number of polyethylene materials of different nature, but also theoretically account for the range of H/E ratios experimentally determined [21].

In the last years, conventional hardness testers, based on the optical measurement of the residual impression, have progressively been substituted by indentation depth-sensing methods. Hardness data derived from the imaging method are mainly related to irreversible plastic processes, i.e., information about the elastic release of the indentation depth is mostly lost. In contrast, continuous depth-sensing indentation monitors the indentation depth as a function of applied load, as the indenter is driven into and withdrawn from the sample surface. Hence, in the latter case, not only plastic but also elastic properties can be derived. Due to the fact that the experimental devices make use of small loads in the mN to nN range, leading to indentation depths within the submicron or even the nanoscale, they are commonly known as nanoindenters. Doerner and Nix [22] proposed the first method to obtain hardness and Young's modulus from nanoindentation data. The method was further developed by Oliver and coworkers [23–25] and it will be shown below that the discussion on the applicability of such method to viscoelastic or visco-elasto-plastic polymers is of the outmost importance.

In recent years, micro- and nanoindentation have been established as a means of detecting a wide variety of morphological and nanostructural changes in amorphous and semicrystalline polymers [26–47], including blends [28], copolymers [32,48], polymer composites [31] and multilayer systems [27]. Dental materials [34], bones [35] and bone analogue biomaterials [36,37], cell nuclei [38], hydrogels [39], polymer composites with carbon nanotubes [40–43] or with organoclays [44,45] and interpenetrating polymer networks [46,47] are some examples of advanced materials that have been extensively studied by means of indentation methods. Micro-indentation has also been proved to be well suited to follow modifications of polymer surfaces produced by ageing or weathering

[49,50], ion implantation [51,52] or various kinds of irradiation such as proton- [53], gamma- [54] or beta-irradiation [55].

This article attempts to summarize some of the most relevant contributions concerning the nanostructure development in polymers, from the glassy state to more ordered structures, by means of indentation hardness. Most of these studies have been carried out using optical microindentation methods. In addition, the last part of the review offers an overview on recent advances in depth-sensing nanoindentation applied to polymer materials.

2. The glassy state

It is well known that microindentation hardness provides direct evidence of changes in the properties of polymer glasses [8,53,54,56–58]. In the glassy state, the critical stress required to plastically deform the amorphous polymer involves displacements of bundles of chain segments against the local restraints of cohesive secondary bond forces and internal rotations [8]. The intrinsic stiffness of these glassy polymers below the glass transition temperature, T_g, leads to microhardness values which may even be 2–3 times larger than those obtained for typical flexible semi-crystalline polymers [59]. On the other hand, according to Gedde [60], T_g generally increases with increasing cohesive energy following a dependence of the type:

$$T_g = 2\delta^2/mR + C_1 \tag{1}$$

where δ^2 is the cohesive energy density, m is a parameter describing the internal mobility of a single chain, R is the gas constant and C_1 is a constant. Several publications have dealt with the existing correlation between the microhardness and T_g for a number of amorphous glassy polymers [61–63]. One obtains a fairly good relationship between H values measured at room temperature (T_{room}) and T_g, in the interval between 300 K and 500 K (see Fig. 1), which can be expressed as [61]:
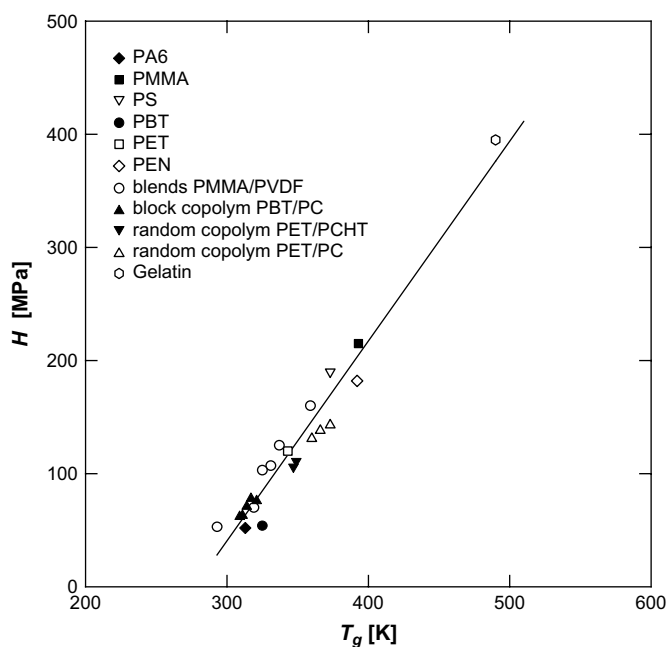
$$H = kT_g + C \tag{2}$$

Fig. 1. Linear correlation between microhardness and T_g for a number of glassy polymers with dominating single bonds in the main chain. Reprinted from Baltá-Calleja FJ, Flores A, Ania F. In: Michler GH, Baltá-Calleja FJ, editors. Mechanical properties of polymers based on nanostructure and morphology, chapter 8, p. 285. Copyright (2005), Taylor and Francis.

where $C = -571$ MPa and $k = 1.97$ MPa/K are experimental fitting parameters. Data of a number of commercial polymers, including polyolefins, polyesters and polyamides, were used in the derivation of Eq. (2). Deviations from the linear relationship found between H and T_g are observed when aromatic rings, or other types of rings, are present in the main chain. Otherwise, for glassy polymers with dominating single bonds in the main chain, Eq. (2) allows to calculate the room temperature hardness values provided the T_g values are known.

2.1. Local order: thermal history and physical ageing

Variations in the average chain packing density in glassy polymers can be readily detected by indentation hardness offering a large advantage over other techniques such as X-ray diffraction. Changes in chain packing density (averaged over a typical volume of 10^2–10^5 μm^3) arise from variations at molecular scale such as conformational rotations, appearance of local order, chain orientation effects, physical ageing, etc. For instance, the internal order in the amorphous state of thin films of polyethylene terephthalate (PET) prepared at different cooling rates from the melt has been studied using the microhardness technique [64,65]. The influence of the cooling rate and physical ageing on H of the glassy samples has been independently discussed [64]. Fig. 2 shows the semilogarithmic plot of H as a function of storage time at T_{room} for PET quenched from the melt at four different cooling rates following the procedure of Piccarolo and coworkers [66,67]: 7500, 700, 178, and 17 °C/s. One observes first a rapid increase of H with time for all the samples during the first month of storage; thereafter, hardness increases at a lower rate. The hardness enhancement observed with storage time is associated with a physical ageing process. Most interesting is the fact that the initial H values depend on the cooling rate used for the preparation of the samples. This finding favours the concept of a different state of internal order for the freshly quenched amorphous samples studied. It is noteworthy that the hardness difference between samples cooled at different rates is retained at long storage times (after more than 1–2 years). Physical ageing involves relaxation towards thermodynamic equilibrium. The molecular mechanisms associated to ageing are still a matter of debate [68]. The results shown in Fig. 2 suggest that differences in the initial structure of the various glassy materials are still apparent after substantial physical ageing. Such differences may arise from local domains with different degrees of internal order, present in the starting un-aged material. These regions could exhibit incipient

molecular ordering, precursors of final crystalline states [65]. Fig. 3 highlights the different hardness values, and concurrent density data, found for PET samples cooled from the melt at different rates in the range 4.7–7500 °C/s and subsequently stored at T_{room} for 40 days [65]. None of these samples exhibit X-ray crystalline peaks. It is noteworthy the increase of hardness with decreasing cooling rate for amorphous PET (increasing ρ values from 1.339 g/cm^3 up to 1.344 g/cm^3). In addition to the above-mentioned data, the figure includes PET samples which were capable to crystallize from the melt ($\rho > 1.35$ g/cm^3) using much lower cooling rates (dT/d$t \leq 2.3$ °C/s). One can clearly distinguish between two regions of behaviour: a fast linear increase of H vs. ρ for the amorphous glassy samples and a second slower linear increase of H vs. ρ for the semicrystalline materials. It is remarkable the steep variation of H (from ≈ 130 MPa up to 155 MPa) for the series of glassy materials showing a density change of less than 4‰.

2.2. Block copolymers and polymer composites

Block copolymers and polymer composites represent possible candidates to reach balanced mechanical properties in a polymer material. Microindentation hardness can be used to study such properties, for instance, as a function of block or filler content. In this section, some recent results of the application of the microhardness technique to the study of blends of a copolymer (glassy and rubbery blocks) and a glassy homopolymer are summarized [28]. In addition, the influence of filler structure on the microhardness of a glassy polymer matrix is highlighted [69].

2.2.1. Influence of styrene content in blends of polystyrene (PS) with a styrene–butadiene–styrene copolymer

The styrene-*block*-butadiene-*block*-styrene (SBS) triblock copolymers were synthesized with the aim of combining the rubbery character of the butadiene blocks with the thermoplastic nature of the styrene ones [70]. The SBS copolymers exhibit two separate T_g values and a microphase-separated morphology whose dimensions lie in the range of the radius of gyration of the molecules [71]. Depending on the molecular architecture of the SBS copolymers, cylindrical or lamellar morphologies can be found [72]. It has been shown that the microhardness of the SBS materials is determined primarily by the different morphology of the separated microphases [72]. Because of their high production costs, the block
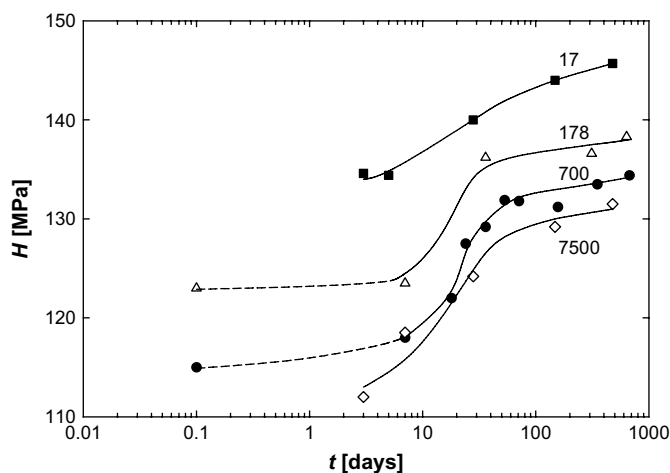

Fig. 2. Variation of hardness with the logarithm of storage time for amorphous PET samples prepared at different cooling rates (in °C/s) from the molten state [28].
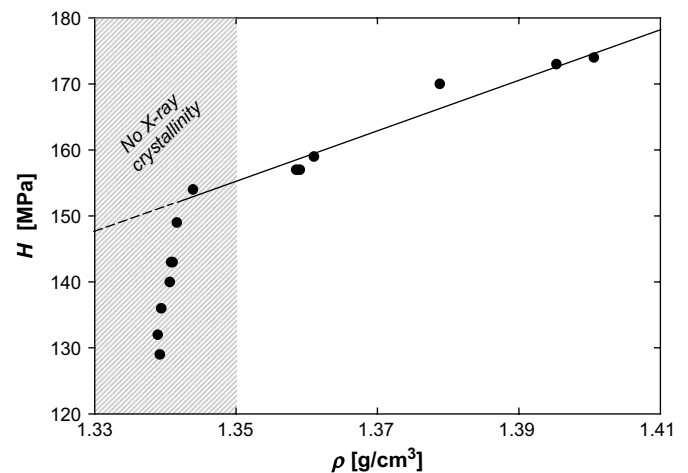

Fig. 3. Variation of hardness for aged PET samples ($\rho < 1.35$ g/cm^3) as a function of density. None of these samples exhibit X-ray crystallinity. Data for crystallized samples of PET ($\rho > 1.35$ g/cm^3), cooled from the melt at much lower rates (dT/d$t \leq 2.3$ °C/s), are also included. Replotted from Ref. [65].

copolymers are seldom used as pure materials, and often prepared in combination with polystyrene homopolymer [70]. The architectural modification of the SBS block copolymers may open new ways of controlling mechanical performance of their blends with polystyrene (PS). Thus, it is of great interest to gain a deeper insight into the structure–property correlations in this type of materials.

Fig. 4 illustrates the variation of the microhardness of injection-moulded bars of blends of PS with SBS, as a function of total PS content (including the styrene content within the copolymer, which is of 74%). The SBS used for the blends is a star block copolymer, with SBS arm structure and PS core. The star block copolymer shows a peculiar lamellar morphology with alternating layers of PS and polybutadiene (PB). By adding the homopolymer PS to the star block copolymer, the thickness of the PS lamellae is continuously increased while the thickness of the butadiene layers remains almost unchanged. The thickness of the PS lamellae varies from 19 nm in the case of SBS copolymer (74% total PS) up to 43 nm when 80% of the homopolymer is added (95% total PS). Fig. 4 (insets) illustrates, as an example, the TEM micrographs of the injection-moulded bars of the two blends. It is seen that not only the PS lamellar thickness (white areas), but also the width of the thickness distribution, increases with increasing PS content.

Fig. 4 shows that addition of the PS homopolymer to the SBS copolymer results in an increase of the total hard phase and hence, an increase in the H values. Preceding studies suggest that the microhardness of amorphous copolymer systems and blends behaves as an additive property of the hardness of the individual constituents [63,73–75]. However, SBS/PS blends exhibit very significant deviations from the additivity law (dashed line in Fig. 4), especially at low PS content. We assume that $H \approx 0$ for polybutadiene, since $T_g \ll T_{room}$, an approximation that finds experimental support in the microhardness measurement of ethylene–octene copolymers with zero degree of crystallinity [32]. This figure also shows that the total PS content in these microphase-separated structures has no linear correlation with the H data and suggests that the lamellar morphology plays a fundamental role in the mechanism of deformation. It has been suggested that the local yield stress for thin lamellae follows a mechanism of deformation, 'thin layer yielding', that would result in a highly ductile behaviour compared to the bulk polymer [76]. This would explain the large
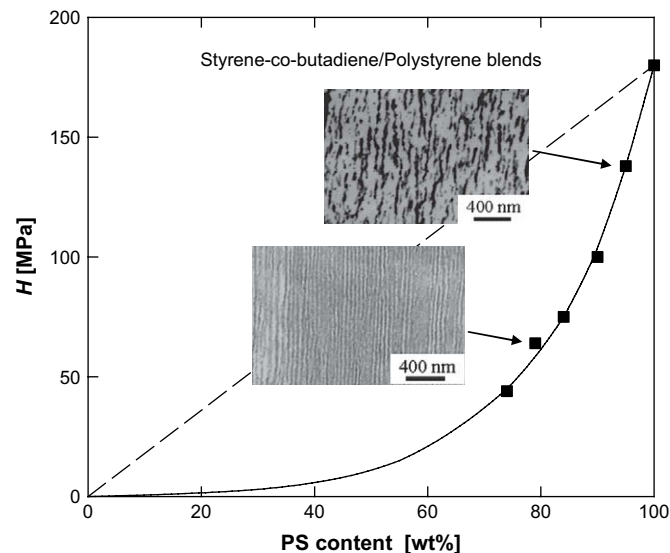
deviation of the microhardness of these materials from the additivity law.

The analogy between the lamellar structures in the blends of SBS and PS with the lamellar crystals in semicrystalline polymers has encouraged the fitting of the data for the amorphous blends to the following equation:

$$H = \frac{H^{PS}}{1 + (K + D_{PS})} \tag{3}$$

where H^{PS} is the hardness of the PS matrix (lamellae with infinite thickness), D_{PS} is the average thickness of the PS lamellae and K is a constant. This constant plays the same role as the parameter b in Eq. (9) (see below) and could be related to the energy of plastic deformation of the PS lamellae. Thus, Eq. (3) is similar to the well experimentally contrasted expression that accounts for the variation of hardness values with crystal thickness for semicrystalline polymers (see Eq. (9), Section 4.2). The representation of $1/H$ vs. $1/D_{PS}$ yields a good agreement of the data to a straight line (results not shown), in agreement with the correlation proposed in Eq. (3), suggesting that the lamellar amorphous block copolymer systems may be regarded, indeed, as an analogue to the semicrystalline systems. Therefore, the enhancement of H values with added PS in the blend (see Fig. 4) could be partly due to an increasing thickness of the PS layers (organized in 'crystalline-like' manner).

2.2.2. Reinforced carbon black composites: influence of filler structure

Earlier research using the indentation test to investigate the micromechanical properties of carbon black–polymer composites was mainly concerned with elastomeric matrice systems [77–82]. Other studies reported on the hardness of carbon black–semicrystalline composites including carbon black filled isotactic polypropylene (iPP) and nylon 6 [83,84].

The microhardness of carbon black–polycarbonate (PC) composites represents an outstanding example with reference to the role of the filler in the nanostructure and resulting micromechanical properties [69]. Two types of microadditives with
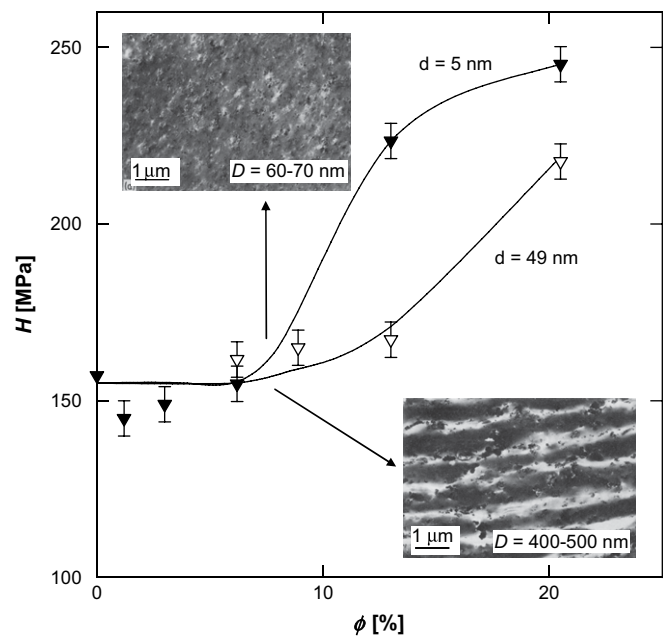

Fig. 4. Hardness of the star block copolymer/PS blends as a function of total PS content. The dashed line represents the hardness additivity law. The insets show TEM images for the two samples with different PS content indicated by arrows. Replotted from Ref. [28].

Fig. 5. Microhardness of PC–carbon black composites against carbon black content for two different particle size values. The insets show TEM images for 6.4% carbon black content with two different agglomerate sizes. Replotted from Refs. [69] and [85].

different average particle sizes were investigated. One having a particle diameter $d = 5$ nm and the other one $d = 50$ nm. Fig. 5 illustrates the plot of the H values vs. the carbon black volume concentration, ϕ, within the polycarbonate samples. The insets of Fig. 5 show transmission electron micrographs of two composite samples with different types of microadditives, at a filler concentration of 6.4% [85]. One of the micrographs shows a homogeneous distribution of aggregates of $D = 60$–70 nm in diameter for the smallest average particle size of the filler; larger dispersed aggregates, 400–500 nm in size, were observed in the other micrograph when incorporating carbon black with $d = 50$ nm.

Fig. 5 shows that, for low carbon black content values ($\phi \leq 6.2\%$), the microhardness of the carbon black–polycarbonate composites is independent of ϕ. It seems that at low filler concentrations, the carbon black aggregates are easily displaced under the indenter. In this case, filler content and particle size do not influence the mechanical properties. It is only above a critical ϕ value, ϕ_H, which depends on the type of carbon black, that the hardness values of the composites conspicuously increase with further increase of filler content. From Fig. 5, values of $\phi_H = 6.2\%$ and $\phi_H = 10$–13% are found for the composites with $D = 60$–70 nm and $D = 400$–500 nm, respectively. Results suggest that the well-developed structure of the more homogeneously distributed carbon black aggregates ($D = 60$–70 nm) hardens the material more effectively. It is noteworthy that the critical filler concentration for hardness enhancement is always significantly higher than that necessary for electrical conductivity (percolation threshold) (results not shown here, see Ref. [69]), suggesting that microhardness is, in this case, less sensitive to filler content than electrical conductivity. Preceding studies have shown that variations in the electrical conductivity of a polymer compounded with carbonaceous fillers do not necessarily involve a parallel change in mechanical properties [86,87]. Indeed, the incorporation of well-dispersed carbon nanotubes into a polyimide matrix was found not to significantly improve the mechanical properties of the polyimide, while the electrical conductivity was raised by more than 11 orders of magnitude at the percolation threshold [86]. In contrast, enhanced mechanical behaviour was found in the case of composites of polyamide-6 and carbon black or carbon nanotubes, already at filler contents below the electrical percolation threshold [87]. It seems that the mechanical properties of electrically conducting polymers, based on a polymer matrix and carbonaceous fillers, are difficult to frame in a general scheme and the final mechanical properties may depend to a large extent on the specimen preparation. In this context, the microhardness technique can serve as a convenient tool to assess the mechanical properties of the polymer composites.

2.3. Microhardness dependence with temperature

In general, the microhardness of amorphous and semicrystalline polymers decreases upon heating due to changes in macroscopic density. It is seen that H follows an exponential decrease as a function of T given by

$$H = H_0 \exp[-\beta(T - T_0)] \tag{4}$$

where H_0 is the hardness measured at a given reference temperature T_0, and β is the so-called coefficient of thermal softening. The β coefficient has been shown to be directly proportional to the temperature dependence of the average molecular cross-sectional area of the crystalline and non-crystalline regions [88]. Data from the literature on glassy polymers show that for $T < T_g$, $\beta \sim (1.2$–$20) \times 10^{-3}$ K^{-1} [89,90]. The β values for semicrystalline materials also lie within the same range [88,91]. On the other hand, for $T > T_g$, H for all polymer materials decreases at a much higher rate yielding $\beta = (22$–$144) \times 10^{-3}$ K^{-1} [89,91].

For glassy materials, a fast H decrease is observed at the glass transition temperature, as early reported for poly(methyl methacrylate) (PMMA), poly(vinyl acetate) (PVAc), glassy PET and glassy poly(aryl ether-ether ketone) (PEEK) [89]. This is due to the onset of liquid-like motions which lead to a much lower cohesive energy density. Fig. 6 illustrates some of these data, together with recent ones reported for PS [26] and PC [92]. In all cases it is shown that H can conveniently detect the glass transition temperature as a bend in the H–T plot. Indeed, a good agreement is found between the T_g values determined from calorimetric studies and those from indention hardness measurements [26,89,90]. It is noteworthy that in the case of PET, we observe an H increase before the sudden drop at T_g. This has been associated with physical ageing, progressively leading to more compact molecular arrangements with reduced free volume [89].

3. Nanostructural development from the glass: influence of confinement

3.1. Development of crystallinity

Certain glassy polymers at T_{room} are capable to crystallize above T_g ($T_g > T_{room}$). A few studies show that one can easily "in situ" follow the kinetics of the crystallization process of a polymer from the glass by measuring the hardness evolution at a given temperature [90,93–95]. Fig. 7 illustrates, as an example, the variation of the microhardness of poly(ethylene naphthalene-2,6-dicarboxylate) (PEN) as a function of crystallization time for various crystallization temperatures [90]. Lower starting H values are found ($t = 0$) for higher crystallization temperatures, in agreement with the hardness tendency to decrease with increasing T. In the course of isothermal crystallization one observes: first an induction time for the crystallization process to start, that is only significant for low crystallization temperatures T_c, secondly a steep H increase, and finally an H levelling-off. The steep H increase, during primary crystallization, is connected with the progressive growth of polycrystalline aggregates (spherulites). When the spherulites impinge with each other, H levels off, and the primary crystallization process finishes. The much slower hardening process is denoted as secondary crystallization and is related with the appearance of new intraspherulitic lamellar stacks, formation of crystals within the interlamellar stacks and crystal thickening.
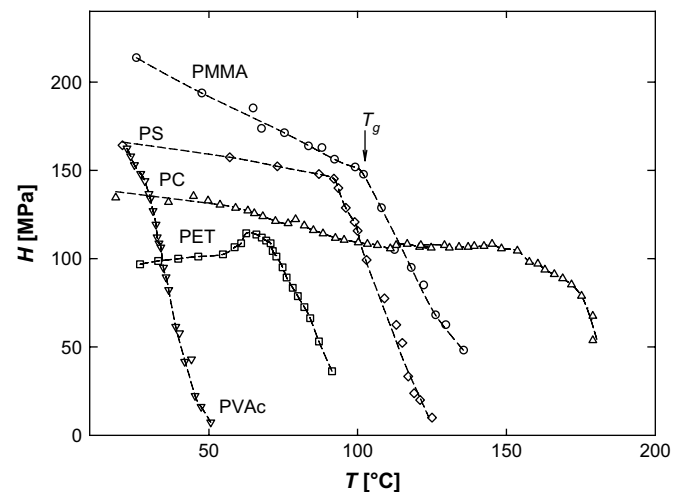

Fig. 6. Microhardness as a function of temperature for a number of glassy polymers: ○, poly(methyl methacrylate) (PMMA) [89]; ◇, polystyrene (PS) [26]; △, PC [92]; □, PET [89]; ▽, poly(vinyl acetate) (PVAc) [89].
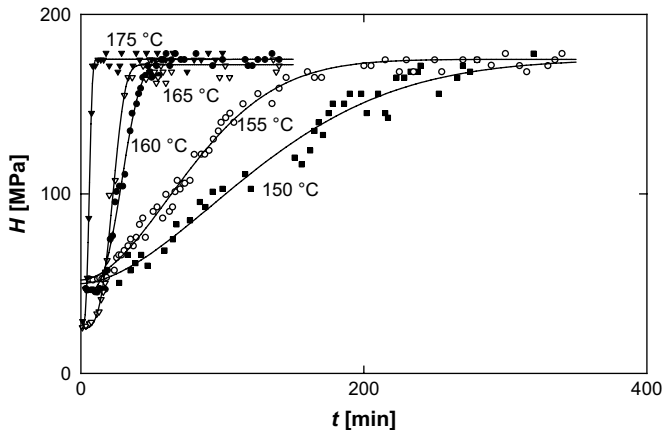
Fig. 7. Variation of microhardness of PEN as a function of crystallization time for various crystallization temperatures: ■ 150 °C; ○ 155 °C; ● 160 °C; ▽ 165 °C; ▼ 175 °C. Reprinted from Polymer, Kajaks J, Flores A, García Gutiérrez MC, Rueda DR, Baltá-Calleja FJ, Crystallization kinetics of poly(ethylene naphthalene-2,6-dicarboxylate) as revealed by microhardness, 41(21), 7769–72. Copyright (2000), with permission from Elsevier.

Room temperature measurements of the hardness variation with the volume fraction of spherulites ϕ during primary crystallization of a number of polymer materials [96–98] yield the following relationship:

$$H = H_{sph}\phi + H_a(1 - \phi) \tag{5}$$

where H_{sph} and H_a are the hardness values of the spherulitic and the amorphous inter-spherulitic regions respectively, characteristic for each polymer material under specific crystallization conditions. Hardness values employed in the derivation of Eq. (5) were obtained from conventional imaging testing. Due to the large volume of deformation involved in the calculation of H ($V > 10^5$ μm³; indentation diagonals reach values of ≈ 100 μm), the mechanical properties of the spherulitic and inter-spherulitic material cannot be discerned. Hence, H_{sph} and H_a are derived from the extrapolation of the linear relationship found between H and ϕ.

On the other hand, hardness values during primary crystallization are shown to be directly proportional to the total emerging crystallinity in the sample [90,93]. This is thought to arise from the direct proportionality between the hardness of the spherulites and the fraction of crystalline material within them, α_L, following [8,96,99]:

$$H_{sph} = H_c\alpha_L + H_a(1 - \alpha_L) \tag{6}$$

Combination of Eqs. (5) and (6) yields:

$$H = H_c\alpha + H_a(1 - \alpha) \tag{7}$$

where H_c is the hardness of the crystals, H_a the hardness of the amorphous regions and α the volume degree of crystallinity. On the derivation of Eq. (7), the hardness of the amorphous intra-spherulitic regions has been assumed to be the same as that of the inter-spherulitic material. However, Eq. (7) can be formulated in a more generalized form, as shown in Ref. [8], by taking into consideration different hardness values for the amorphous intra- and inter-spherulitic material.

Eqs. (5)–(7) suggest that the microhardness of a polymer material is an additive property of the hardness of the crystalline and amorphous phases. All of these equations were initially proposed to explain certain experimental observations and represent nowadays well-established correlations with sound experimental evidence [30,90,93,94,96–98,100–111].

The direct proportionality between hardness and degree of crystallinity allows deriving information on the kinetics of crystallization from indentation experiments. Indeed, Avrami analysis of the crystallization curves in Fig. 7 yields n values around 2 for the lowest crystallization temperatures ($T_c \leq 155$ °C) while $n \sim 3$ within the range 160 °C $\leq T_c \leq 175$ °C. Results are consistent with transmission electron microscopic investigations on the morphology developed during isothermal crystallization of PEN from the glassy state [112].

3.2. Influence of confinement on the kinetics of crystallization

New materials are being developed as nanotechnology extends the limits of fabrication to the nanoscale. The structure–property relationships are best understood when the hierarchical nature of the system is taken into account, i.e., the structural organization in discrete levels held together by specific interactions of the components [113]. The physical properties in polymeric layered systems, such as the glass transition temperature, crystallizability and toughness, are altered by reducing the layer thickness down to a few tens of nanometers [76,114–116]. By using layer multiplying co-extrusion, a wide variety of polymer systems with thousands of layers have been developed in the last years for the most various applications: narrowband 1D photonic crystals, polymer films for surface emitting lasers, membrane and gas barrier structures, etc. [117,118]. These systems also offer the opportunity to examine the influence of physical confinement during nanostructure development on the micromechanical properties.

Fig. 8 (top) illustrates typical indentations made on the PET and the PC layers of the starting 50/50 PET/PC multilayer system, with layer thickness of 59 μm [27]. The darker areas correspond to PC. A similar area of indentation (applied load is 0.02 N) is found for both PC and glassy PET, and hence, similar hardness values are obtained
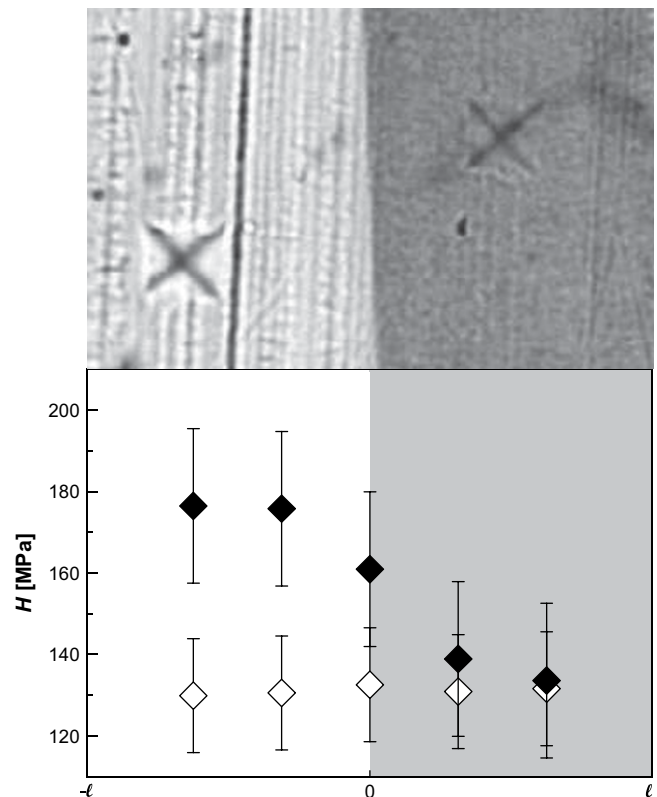

Fig. 8. Top: Micrograph of typical indentations made on adjacent PET/PC microlayers. The darker area corresponds to PC. Bottom: Microhardness values across the interphase of the layers as processed (◇) and after annealing (◆). Replotted from Ref. [27].

(Fig. 8 bottom). However, for the annealed samples ($T_c = 150\,°C$, $t = 25\,min$), H increases in the PET layers and a transition from the harder crystallized PET layer to the less hard PC component is observed across the layer thickness.

In-situ microindentation measurements have been employed to follow the nanostructure development within the PET layers, as a function of layer thickness [92]. Fig. 9 shows the microhardness variation during isothermal crystallization at 117 °C for various 50/50 PC/PET multilayer systems with different PET layer thicknesses: 32, 1 and 0.25 μm. In this case, the load (0.05 N) was applied perpendicularly to the surface layers. The indentation size was such that the volume of deformation involved both polymer materials. This was confirmed by making indentations on both outer layers (PET and PC) that were found to be indistinguishable from each other [92]. Fig. 9 shows that as the layer thickness decreases (increasing confinement): (1) the variation of hardness with time during primary crystallization slows down, and (2) the final levelling-off value decreases. The hardness decrease observed with decreasing layer thickness is in consonance with the sharp decrease of crystallinity for layer thicknesses below 1 μm reported in X-ray diffraction studies of the same multilayer systems [119]. In other words, the physical confinement in the crystallizable polymer nanolayers leads to a strong depression of the crystalline fraction and consequently to a notable decrease in the final mechanical properties.

4. Nanostructure–microhardness correlations for the semicrystalline polymer

In the preceding section, we have shown the potential of the microhardness technique to in situ follow the kinetics of crystallization. At the heart of this ability underlies the intimate correlation between the microhardness and the nanostructure of a polymer material (see Sections 4.1 and 4.2, Figs. 10 and 11). A number of papers provide a sound experimental evidence of the linear relationship between microhardness and the degree of crystallinity of a polymer material [30,90,93,94,96–98,100–111]. A parallel model of crystalline and amorphous layers appears to describe the response of a polymer material to a local deformation, as described in Eq. (7). Crist reported that spherulite size does not directly influence the yield behaviour in polyethylene (PE) [59]. Eq. (7) has broadly demonstrated to apply to polymer systems with T_g values well above the temperature of measurement, in other words, with
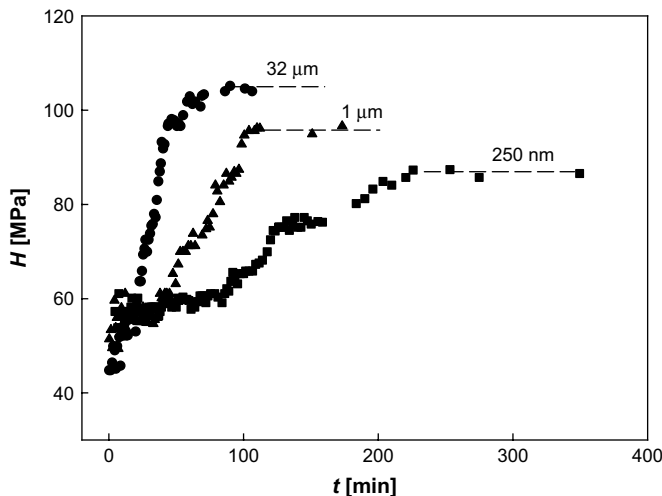
Fig. 10. Microhardness as a function of degree of crystallinity α for a number of polymer materials: ◇, linear PE [101,102]; ● and ○, isotactic PP in the β- and the α-crystalline phases respectively [100,103]; ▽, poly(butylene terephthalate) (PBT) in the α-form [48,104,105], a small percentage of the β-form (4%) is present in the sample with $H = 153$ MPa and $\alpha = 0.47$ [105]; □, PET [30,106,107]; ▼, atmospheric crystallized PEN [98,108] and high-pressure crystallized PEN [108].

amorphous regions in the glassy state. In addition, this equation also holds for polymer systems exhibiting relatively large degrees of crystallinity ($\alpha > 0.3$), in spite of their T_g being below or in the vicinity of the temperature of measurement. In this case, the hardness of the amorphous regions is well described assuming $H_a \approx 0$ and Eq. (7) simplifies to:

$$H \sim H_c \alpha \qquad (8)$$

This section is devoted to polymer systems with H that conforms to Eq. (7) or (8). In the next section, the microhardness behaviour at room temperature of polymer systems, with low degree of crystallinity and $T_g < T_{room}$, exhibiting large deviations of H from the microhardness additivity law will be discussed.

4.1. Dependence with the degree of crystallinity

Fig. 10 illustrates the variation of microhardness as a function of the degree of crystallinity for various polymer systems. Data are taken from Refs. [30,48,98,100–108] and were selected to represent

Fig. 9. Influence of layer thickness on the microhardness of PET layers from PET/PC films during an isothermal crystallization at 117 °C. Replotted from Ref. [92].
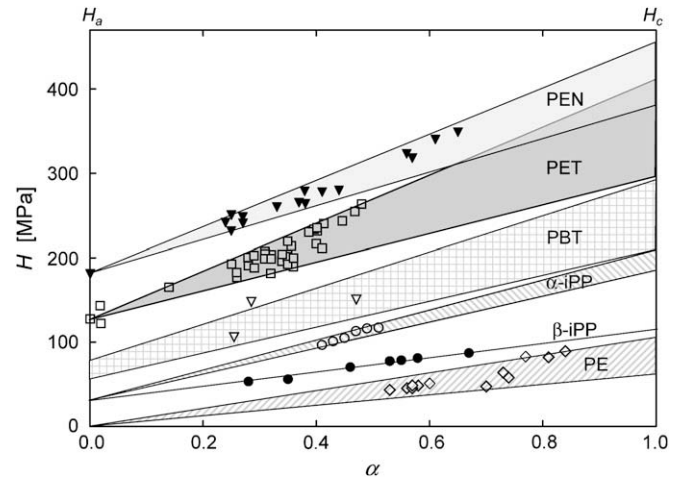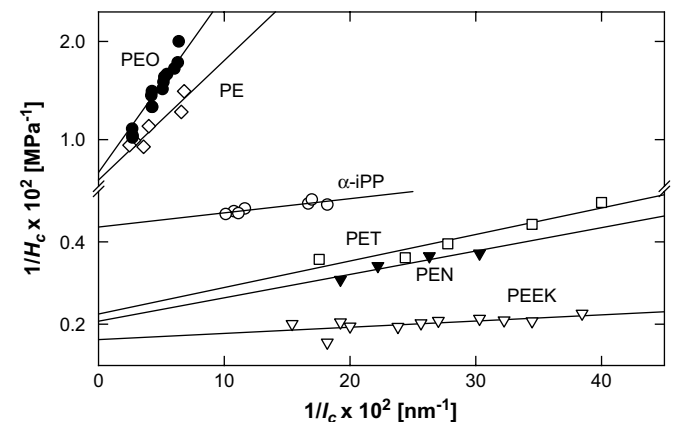
Fig. 11. Reciprocal of the crystal hardness as a function of reciprocal of the crystal thickness for a range of polymer materials, from flexible polyolefins to semirigid polyesters: ●, PEO [122]; ◇, linear PE [102]; ○, iPP in the α-form [100]; □, PET [74]; ▼, PEN [98]; ▽, PEEK [109].

polymer systems with different degrees of rigidity in the main chain. In the first place, it is clearly seen that the range of microhardness values that each polymer exhibits is mainly determined by the nature of the molecular chain. Indeed, PEN exhibits the largest cohesive energy density within the amorphous regions and the strongest intermolecular forces holding the molecules within the crystals, and hence, the resistance to plastic deformation is the highest of all the series. In addition, for each polymer system, the microhardness values cover a wide range, with a tendency to increase with increasing degree of crystallinity. We learn from Eq. (7) that if only the degree of crystallinity were modulating the microhardness values, then, a plot of the *H* vs. *α* values should lie in a straight line, the left-hand and right-hand *y*-axis intercepts representing H_a and H_c respectively. However, a wide range of *H* data is clearly seen in Fig. 10 for nearly all polymer materials. This is a consequence of other nanostructural features, such as the crystal thickness, not taken into account so far, that also contribute to the microhardness behaviour.

4.2. Influence of crystal thickness

The influence of crystal thickness on the microhardness values of polymer materials was first reported in the late seventies [120]. A few years later, on the basis of a heterogeneous deformation model involving the heat dissipated by the plastically deformed crystals, Baltá-Calleja and Kilian developed an approach to calculate the dependence of hardness on the average crystal thickness [121]. According to this model, the crystal hardness (heat dissipated by the crystals) is proportional to the ratio of the enthalpy of crystal destruction to the volume of crystals destroyed. In turn, the crystal hardness dependence with crystal thickness l_c is given by:

$$H_c = \frac{H_c^\infty}{1 + \dfrac{b}{l_c}} \qquad (9)$$

where H_c^∞ is the hardness of an infinitely thick crystal (maximum possible value of dissipated energy through plastic deformation) and *b* is a parameter related to the surface free energy σ_e of the crystal and to the energy *Δh* required for plastic deformation of the crystals through formation of a great number of shearing planes ($b = 2\sigma_e/\Delta h$). H_c^∞ is mainly related to the chain packing density within the crystals and represents the upper limit to the hardness of a polymer material. It is noteworthy that H_c^∞ determines to a great extent the range of microhardness values shown for each polymer in Fig. 10. In addition, the crystal thickness values (and to a lesser extent the *b* parameter) also modulate the microhardness values. Indeed, the data shown in Fig. 10 suggest that there is no unique straight line for each polymer material that could account for a hardness enhancement as the degree of crystallinity increases, but rather a variety of straight lines (each shaded area in Fig. 10) with a common H_a value and a range of H_c values (right-hand *y*-axis intercepts), the latter mainly determined by the crystal thickness. With the help of Eqs. (7) and (9), one can fully account for the micromechanical properties of a polymer system, based on the detailed nanostructure.

A number of studies have supplied experimental support to Eq. (9). Fig. 11 illustrates the plot of $1/H_c$ as a function of $1/l_c$, for various semicrystalline polymers. The *y*-axis intercept yields $1/H_c^\infty$. It is noteworthy that the semirigid polyesters (PET [74] and PEN [98] and PEEK [109]) exhibit higher H_c^∞ and smaller l_c values than those for the flexible polyolefins (iPP [100], PEO [122] and PE [102]). Table 1 collects the H_c^∞ values derived from Fig. 11, together with additional H_c^∞ data, not included in this figure for the sake of clarity [97,75,123].

Table 1
H_c^∞ for various polymer materials.

| Polymer	H_c^∞ [MPa]
*i*PBu-1 (II)	27 [123]
*i*PBu-1 (I)	104 [123]
PEO	150 [122]
PE	170 [102]
*i*PP (α-form)	230 [100]
PBT	370 [75]
PET	400 [74]
PEN	500 [98]
TPI	≈500 [97]
PEEK	615 [109]

4.3. Creep behaviour

A comprehensive understanding of the micromechanical properties of polymer materials should necessarily include a study of their visco-elasto-plastic character. Depth-sensing instrumentation provides the possibility to record the elastic as well as the plastic properties and hence, to extract the visco-elasto-plastic response of the polymer material from the indentation curves. A number of approaches have been developed to extract creep properties from depth-sensing instrumentation, the nature of which is diverse, including phenomenological approaches, semi-empirical models and linear viscoelasticity assumptions at small strains [124–130]. However, so far, there is no widespread methodology to analyze creep data from depth-sensing instrumentation and hence, comparison of the creep properties of different polymeric materials is difficult to achieve. In contrast, it is a common practice to use phenomenological approaches to describe the time-dependent behaviour of microhardness, derived from conventional testing (optical method). In this case, creep is related to the visco-plastic properties of the material and is commonly described following [64,88,91,109,131–137]:

$$H = H_1 \Delta t^{-k} \qquad (10)$$

where H_1 is the hardness at a given reference indentation time $\Delta t = 1$ and *k* is a parameter (creep constant) which gives the rate at which the material flows under the indenter. The decreasing power law function of Eq. (10) was first adopted for polymer materials in the early eighties [138], after Mulhearn and Tabor had proposed a similar expression to describe the variation of hardness as a function of indentation dwell time for soft metals [139]. Fig. 12 illustrates the range of creep constant values reported for a wide variety of polymer materials. A number of observations can be drawn: 1) Glassy materials creep at a higher rate than the crystallized ones; as an example, the *k* value of glassy cold-drawn PET is higher than that of the crystallized cold-drawn sample. 2) Inorganic reinforced polymers creep at a lower rate than the matrix itself, as revealed by the *k* data of an acrylic terpolymer and that of the same material reinforced with titania particles. 3) The inclusion of 'soft' rubbery particles in a polymer matrix (such as Core–Shell rubber Particles in PMMA) yields larger *k* values. 4) The creep constant is dramatically affected by the temperature of measurement; as an example, the *k* parameter of PMMA at 90 °C doubles the value at T_{room}, and that of CEPE at 123 °C is three times the *k* value at T_{room}. 5) Polymer materials with large hardness values usually exhibit the smallest *k* values. However, polyethylene materials represent an intriguing exception to this rule. One can see that the ethylene–octene copolymer, EOC (degree of branching of 5%), not only flows at a lower rate under the indenter of all the PE-based materials, but also exhibits one of the smallest *k* values of all polymer materials, close to those reported for glassy drawn PET and for poly(6-oxy-2-naphthoate) (PHN); on the other hand, EOC displays a remarkably

Creep constant, k [10^{-2}]
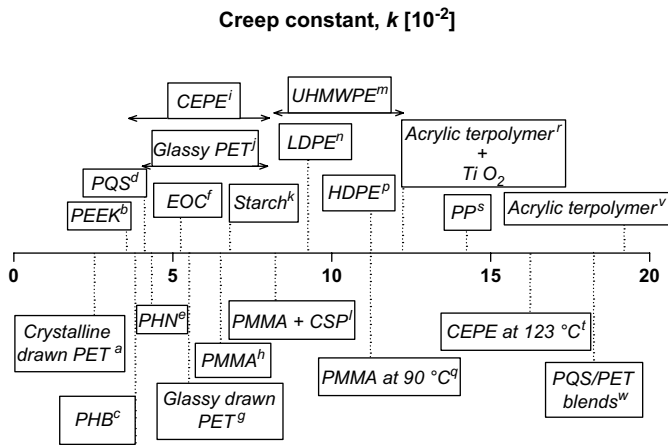
Fig. 12. Creep constant at room temperature (except otherwise stated), for the following polymer materials: *a*) PET crystallized from the oriented glassy state [132]; *b*) PEEK crystallized from the glass [109]; *c*) poly(4-hydroxybenzoate) (PHB) [88]; *d*) poly(phenylene sebacate) (PQS) [131]; *e*) poly(6-oxy-2-naphthoate) (PHN) [88]; *f*) EOC with 5% branching content (unpublished results); *g*) glassy drawn PET [132]; *h*) PMMA [133]; *i*) chain-extended polyethylene (CEPE, crystallized or annealed at high pressure) [91]; *j*) isotropic glassy PET [64]; *k*) thermoplastic starch [134]; *l*) PMMA with core–shell rubber particles [133]; *m*) ultra-high molecular weight polyethylene (UHMWPE) [91]; *n*) low density polyethylene (LDPE) [135]; *p*) high density polyethylene (HDPE) [91]; *q*) PMMA, *k* was measured at 90 °C [133]; *r*) polyacrylic titania hybrid, the acrylic polymer is a random terpolymer of methyl methacrylate (MMA), *n*-butyl methacrylate (BMA) and methacrylic acid (MA) [136]; *s*) polypropylene (PP) [135]; *t*) CEPE, measured at 123 °C [91]; *v*) P(MMA-BMA-MA) terpolymer [136]; *w*) PQS/PET blends [131].

low hardness value ($H = 0.53$ MPa). In addition, the k value of low density PE (LDPE) is clearly lower than that of high density PE (HDPE). We believe that this behaviour must be a consequence of the density of entanglements in the amorphous phase due to the presence of branches. As the material is compressed under the indenter, branching would enhance the formation of new entanglements and the reinforcement of the existing ones, which could act as physical links against the material deformation.

5. Mechanisms of deformation

5.1. Elasto-plastic behaviour below T_g

The validity of Eq. (7) to describe the micromechanical properties of a number of polymer materials relies on the fact that plastic deformation takes place in both the crystalline and the amorphous regions. This is indeed the picture for T_{room} measurements of polymer materials with $T_g > T_{room}$. In this case, the stress applied is effectively transferred to both the amorphous and the crystalline regions. The distribution of stresses in the deformed volume is determined by the geometry of the indenter and it is only above a critical stress level that the material undergoes plastic yielding [17,11]. The volume of irreversible deformation is typically associated to 4–10 times the residual indentation depth in the direction perpendicular to the contact surface. Beyond this boundary, only elastic deformation takes place.

During an indentation cycle, the material is subjected to a compressive stress that induces a structural rearrangement on the polymer material. At small applied stresses, bond rotations and lamellar shearing are envisaged; higher stresses could lead to chain scission and lamellae fracture. The detailed mechanisms of deformation are still unclear and mostly based on indirect evidence. In recent years, a novel synchrotron radiation set-up allowing for simultaneous microdiffraction and microindentation experiments has been successfully developed [140–142]. An X-ray beam with a cross-section of a few micrometers has been used to "in situ" probe the vicinity of the indenter during a microhardness test.

Combined microindentation and microdiffraction in polymer fibres suggest that the nanostructural changes occurring upon both elastic and plastic deformation are mainly associated with a perturbation of the orientation of the crystal blocks, clearly distinguished upon loading and partly retained after the tip withdrawal. In addition, it has also been shown that the stress field under the indenter may induce a polymorphic transformation [140–142].

5.2. Low crystallinity systems with elastomeric character

The mechanisms of deformation taking place upon indentation of polymer materials with a marked elastomeric character should be substantially different from those described in the preceding section. This mainly refers to experiments carried out at T_{room} in polymers with $T_g < T_{room}$ and showing low crystallinity values. In such systems, the crystallites are immersed in a viscous amorphous phase which is predominant in the material. Hence, the interaction between the amorphous 'soft' material and the 'hard' crystallites is envisaged to play a fundamental role in the modes of deformation. Indeed, it is often observed that the microhardness values of such systems deviate to a great extent from the additivity law [32,48,143,144]. Two systems have been chosen to illustrate such behaviour: i) a series of ethylene–octene copolymers [32] and ii) a range of ester–amide copolymers [48].

5.2.1. Ethylene–octene copolymers

Table 2 collects the branching content and the crystallinity values, determined from density measurements, of the series of ethylene–octene copolymers (EOC) investigated. The table shows the gradual decrease of crystallinity detected with increasing branching content, reaching for the highest branched sample the value of $\alpha = 0$. Most interesting is the fact that the microhardness decreases to values as low as $H = 0.12$ MPa, for the sample with the highest branching content. The validity of the assumption of the microhardness value for amorphous material above T_g to be close to zero (Eq. (8)) is now experimentally demonstrated. It is noteworthy that the largest H value for the ethylene-1-octene series (13 MPa for 1.2% degree of branching) is substantially smaller than the typical values for linear PE samples (43–90 MPa) [101,102]. Fig. 13 shows the variation of the microhardness of the EOC series as a function of the degree of crystallinity. Characteristic data for linear polyethylene have been also included for comparison. Typical H_c values for linear PE range from 67 to 106 MPa. These H_c values satisfactorily correlate with the lamellar thickness ($l_c = 11$–40 nm) according to Eq. (9). However, H for the low crystallinity copolymer samples follows a different trend with α as that shown for linear PE. If one assumes the microhardness additivity law of the individual phases (Eq. (8); $H_a \approx 0$), then, H_c values in the range of 7–32 MPa

Table 2
Branching content, density, crystallinity from density (α), crystal thickness (l_c), microhardness (H) and crystal hardness (H_c) values at T_{room} of ethylene-1-octene copolymers. Reprinted from Polymer, Flores A, Mathot VBF, Michler GH, Adhikari R, Baltá-Calleja FJ, Novel aspects of microindentation hardness in very low crystallinity ethylene-1-octene copolymers: A model for deformation, 47(15), 5602–9. Copyright (2006), with permission from Elsevier.

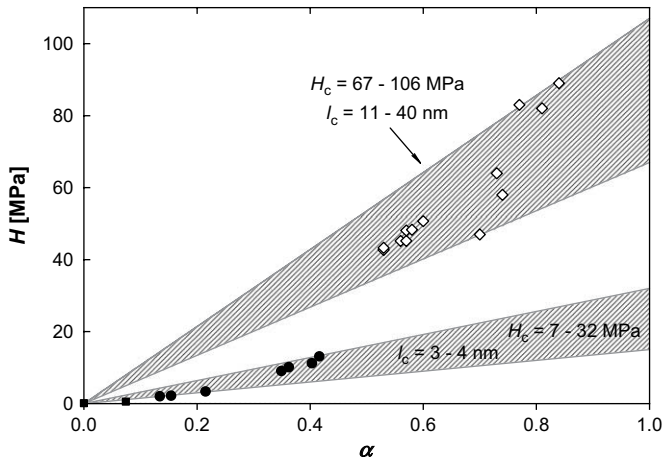| Sample	CH$_3$/100C	ρ [g/cm^3]	α	l_c [nm]	H [MPa]	H_c [MPa]
EOC1	1.24	0.910	0.416	4.5	13.1 ± 0.1	31.5
EO2855M	1.92[FTIR]	0.908	0.403	3.9	11.2 ± 0.3	27.8
EOC2	2.20	0.902	0.362	3.5	10.1 ± 0.1	27.9
EO2711M	2.36[FTIR]	0.900	0.349	3.3	9.05 ± 0.08	25.9
EOC3	3.14	0.868	0.134	3.1	2.0 ± 0.2	14.9
EO2835M	3.59[FTIR]	0.880	0.215	3.1	3.4 ± 0.1	15.6
EO2741M	4.21[FTIR]	0.871	0.154	3.0	2.18 ± 0.01	14.2
EO2963M	5.08[FTIR]	0.859	0.074	3.0	0.53 ± 0.02	7.2
EO4082M	6.00[NMR]	0.848	0.00	–	0.12 ± 0.02	–

Fig. 13. Microhardness variation with degree of crystallinity α for the series of ethylene-1-octene copolymers (solid symbols). Data for linear PE are included for comparison (open symbols) [101,102]. Reprinted from Polymer, Flores A, Mathot VBF, Michler GH, Adhikari R, Baltá-Calleja FJ, Novel aspects of microindentation hardness in very low crystallinity ethylene-1-octene copolymers: A model for deformation, 47(15), 5602–9. Copyright (2006), with permission from Elsevier.

are obtained. The remarkably low H_c values obtained for the highest branched materials ($H_c \approx 10$–15 MPa, see Table 2) cannot be accounted for as due to small crystal thickness values ($l_c \approx 3$ nm), and one should invoke variations in the b parameter (see Eq. (9)).

Fig. 14 (lower curve) shows the b values, calculated using Eq. (9), as a function of branching content, for the ethylene-1-octene copolymers. The range of b values typical for linear PE is also included for comparison [101,102]. The conspicuous increase of the b values above 2% branching could be related to: i) an increase in the surface free energy of the crystals (σ_e) due to a gradual transformation of the lamellar morphology into a granular blocky structure, found in the EOC series as the branching content increases [145]; ii) a change in the enthalpy associated to the modes of deformation, Δh. To shed more light on this issue, let us recall the existing analogy between the hardness equation and the Thomson–Gibbs equation [32]:

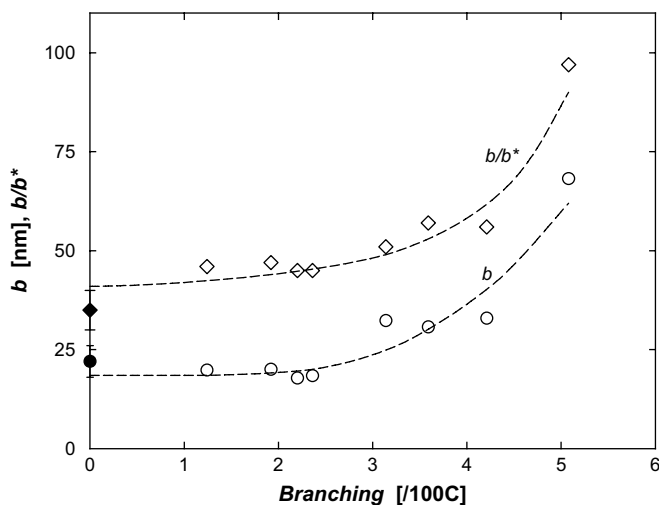$$T_m = T_m^\infty \left(1 - \frac{b^*}{l_c} \right) \tag{11}$$

Fig. 14. Plot of the b parameter (bottom) and of the ratio between b and the thermodynamical b^* parameter (top), as a function of short-chain branching content for the EO materials (open symbols). The typical b values for linear PE are also included (solid symbols) [101,102]. Replotted from Ref. [32].

where T_m^∞ is the equilibrium melting point and $b^* = 2\sigma_e/\Delta h_f$, Δh_f being the melting enthalpy. It is to be noted that b^* relates to the thermodynamical properties while b depends on the mechanical behaviour. Consequently, the study of the b/b^* ratio ($b/b^* = \Delta h_f/\Delta h$) as a function of branching content offers the opportunity to disregard the influence of σ_e and study the changes of Δh. Fig. 14 illustrates the significant increase of the ratio b/b^* (upper curve) as a function of branching content, especially above 2% branching. This result suggests that the energy required for plastic deformation Δh is substantially smaller for the highly branched materials. For low levels of crystallinity ($\alpha = 0.07$–0.22), the small and imperfect nanocrystals are dispersed within a viscous amorphous phase ($T_g \approx -65$ °C). Hence, in these low crystallinity systems, the nanocrystals supposedly 'slide' easily within the amorphous matrix under the influence of the compressive stress of the indenter. This different mode of deformation is manifested in a low Δh value that, eventually, would explain the low H values found.

For materials with degree of branching <3%, the levels of crystallinity already reach al least around 35% and the presence of nanocrystals randomly distributed within the amorphous phase constitutes a network of physical crosslinks connected by bridging molecules that induce a significant reinforcement of the material. In this case, Eqs. (7) and (9) account for the range of H values observed, the Δh values being in the range of those experimentally observed for other linear PE samples. The small crystal thickness is here the feature that limits the material resistance to plastic deformation.

5.2.2. Random polyester–amide copolymers

The deformation mechanisms of a polymer above T_g during indentation can be further understood in the light of a microhardness study carried out in a series of random ester–amide copolymers based on butyl terephthalate and an etherdiamide [48]. These materials possess a hetero-phase structure, with two T_g values and only one melting temperature above room temperature which corresponds to the fusion of poly(butylene terephthalate) (PBT)

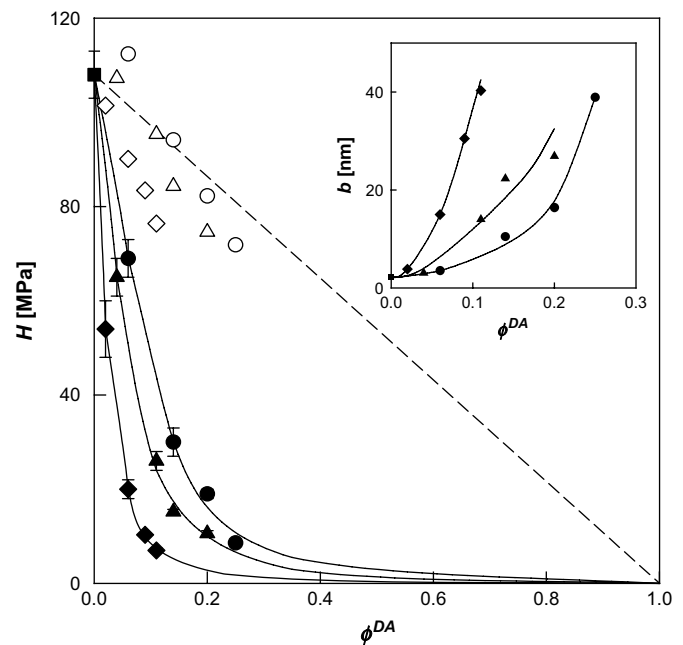**Fig. 15.** Plot of the microhardness values (solid symbols) and calculated H data (open symbols) as a function of etherdiamide content for the PBT homopolymer (■) and the copolyester amides of different molecular weight: $M_n = 750$ g/mol (●, ○); $M_n = 1100$ g/mol (▲, △); $M_n = 2100$ g/mol (◆, ◇). The inset shows the b-parameter values for the same copolymer materials. Replotted from Ref. [48].

crystals. The diamide segments are chosen to mainly contribute to the amorphous domains and confer to the material an elastomeric character.

Fig. 15 illustrates the variation of the microhardness values (solid symbols) as a function of the etherdiamide content, ϕ^{DA}, for all the copolymers investigated. The different symbols represent materials with different molecular weights arising from a different length of the etherdiamide sequence. The H value of the PBT homopolymer is also included in the figure. Hardness is shown to drastically decrease with increasing etherdiamide content. Preceding studies suggest that the microhardness of copolymer materials behaves as an additive property of the hardness of the individual components [8]. In the case of the random polyester–amide copolymers:

$$H = H^{PBT}\left(1 - \phi^{DA}\right) + H^{DA}\phi^{DA} \tag{12}$$

Here, H^{PBT} and H^{DA} are the hardness values of the PBT and etherdiamide components respectively. This equation is described by a straight dashed line in Fig. 15, where we assume $H^{DA} \approx 0$, since T_g of the polyetherdiamide homopolymer is far below T_{room}. It is seen that the hardness values of the copolymers clearly deviate from the linear additivity law. The magnitude of this deviation is larger the higher the molecular weight of the copolymer is (the longer the etherdiamide sequence); that is, the stronger is the elastomeric character of the material.

Let us attempt to explain the hardness values in Fig. 15 on the basis of changes in the degree of crystallinity and crystal thickness of the PBT crystals. The degree of crystallinity for the copolymer series decreases as the etherdiamide content increases, within the range $\alpha = 0.3$–0.15, the crystal thickness remaining constant for all etherdiamide contents and molecular weights ($l_c \approx 6.5$ nm) [48]. The open symbols in Fig. 15 represent the hardness values calculated with the help of Eqs. (7), (9) and (12) (assuming $H^{DA} \approx 0$), using the values of the degree of crystallinity and the crystal thickness of PBT in each copolymer sample. It is further assumed that the b value for the PBT crystals in the copolymer material is the same as that of the PBT homopolymer crystallites. The difference between the calculated and the experimental values is remarkable and suggests that, similarly to the case of the EOC, the hardness of the butylene–diamide copolymers cannot be explained only on the basis of the detailed nanostructure and one needs to invoke large values of the b parameter. Indeed, the inset of Fig. 15 illustrates the behaviour of the b parameter as a function of etherdiamide content, for the copolymers with different molecular weights. A clear rise in the b parameter as the etherdiamide content increases can be observed. Moreover, the b/b^* ratio behaves in a similar way, increasing as the diamide content increases (plot not shown; see Ref. [48]). Results suggest that the enthalpy of deformation Δh decreases with increasing diamide content, as a consequence of the occurrence of deformation modes characteristic of elastomeric materials, similarly to those described for the EOC copolymers.

In summary, polymer materials with elastomeric character (low crystallinity values, $T_g < T_{room}$) exhibit hardness values far below the linear additivity law predictions. We believe that this result is mainly due to the different modes of deformation for elastomeric polymers, with respect to polymer materials with $T_g > T_{room}$. In the former, crystallites are dispersed in a viscous amorphous material in a minor amount and 'slide' within the amorphous matrix upon indentation. The extent of the 'slippage' mechanism should be modulated by the viscosity of the amorphous phase. This mode of deformation is apparent in the high b values determined for this type of materials, a finding that is directly related with the low energy required for this mechanism of deformation.

In recent years, Fakirov has developed a different approach to account for the effect of the above-mentioned 'slippage'

mechanism on the microhardness values of polymers with elastomeric character ($T_g < T_{room}$) [146]. An additional term is introduced in Eq. (8), meant to represent the 'effective' hardness H_a of the soft amorphous phase. In this approach, H_a exhibits negative values which are determined from Eq. (2) that was, however, originally derived from data of a number of glassy materials ($T_g > T_{room}$). Although the hardness values calculated in this way agree fairly well with the experimental ones, this method makes use of negative hardness values which do not have a sound physical meaning.

6. Precursors of crystallization in oriented systems: the smectic-like phase

In the preceding sections, the deformation mechanisms under the indenter, in the case of isotropic polymers are discussed. The following question arises: How can we correlate microhardness with nanostructure for oriented materials? How does the structure development proceed in this case?

The average molecular orientation of a polymer material can be readily detected by means of indentation hardness. For uniaxially oriented polymers, the residual impression after load release shows anisometric diagonal lengths [6]. $H_{\parallel}$ and $H_{\perp}$ are defined as the hardness values derived from the diagonal lengths parallel and perpendicular to the direction of preferential orientation respectively. The indentation anisotropy, ΔH, is defined as [6,137]

$$\Delta H = 1 - \left(H_{\perp}/H_{\parallel}\right) \tag{13}$$

where $H_{\perp}$ is related to the plastic deformation modes of the material and the larger $H_{\parallel}$ values arise from the instant elastic recovery in the chain direction. It has been shown that ΔH is a suitable parameter for measuring the preferred chain axis orientation [6]. Indeed, a linear empirical correlation has been found between ΔH and the optical birefringence Δn for injection-moulded oriented PE [147].

6.1. The oriented glassy material

Glassy polymers may be drawn through neck formation at T_{room} [1]. In the case of PET, the drawn material is highly oriented, however it does not exhibit any crystalline order as shown by Göschel [148].

Fig. 16 illustrates the wide-angle X-ray scattering (WAXS) pattern of a cold- (left-hand side) and of a hot- (right-hand side) drawn PET sample. Cold drawing was carried out at T_{room} (25 °C), while hot drawing was performed at 90 °C. For cold-drawn PET, a strong equatorial maximum can be clearly distinguished together with several layer lines on the meridian and no trace of crystalline reflections. The meridional maxima can be associated to the highly oriented nematic-like structure [149]. In contrast, the WAXS pattern of hot-drawn PET displays a diffuse broad ring with a slightly higher intensity around the equator which suggests that molecules in the hot-drawn sample are poorly oriented along the drawing axis. Similar to cold drawing, no significant crystallinity is observed.

Table 3 illustrates the microhardness values measured perpendicular and parallel to the draw direction and the corresponding indentation anisotropy values for cold- and hot-drawn PET [33]. Values for a hot-drawn PMMA sample have also been included [150]. Hot-drawn PET does not exhibit significant indentation anisotropy, in agreement with the nearly isotropic WAXS pattern shown in Fig. 16. In contrast, cold-drawn PET and hot-drawn PMMA exhibit larger $H_{\parallel}$ values than those of $H_{\perp}$. As mentioned above, this is a well-known behaviour due to the instant elastic recovery of the material along the chain direction that in the case of drawn PET has been associated to the elastic response of the molecules located
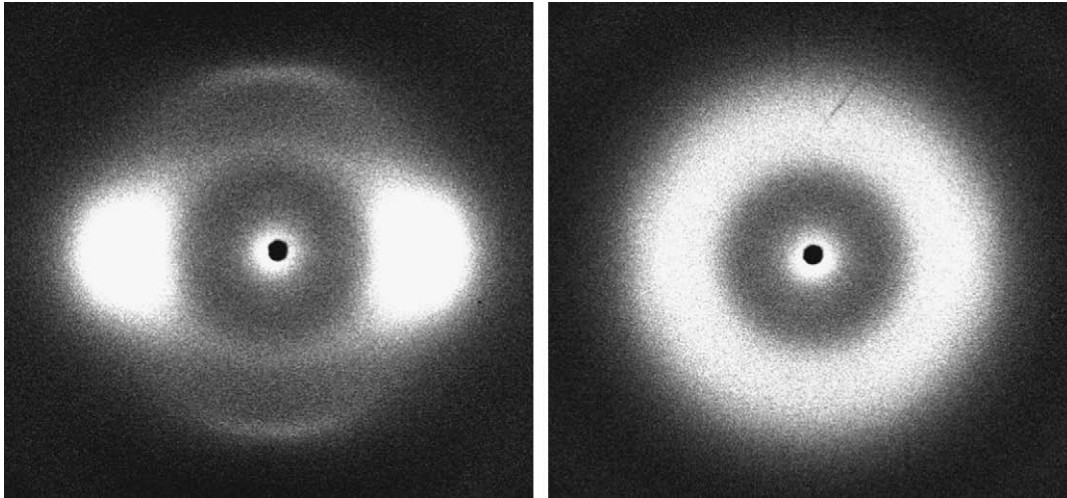
Fig. 16. WAXS pattern of the unannealed cold- (left) and hot- (right) drawn PET samples. Replotted from Ref. [33].

within the amorphous regions. Most interesting is the fact that typical hardness values for isotropic systems (see $\langle H \rangle$ in Table 3) are always significantly larger than $H_\perp$, especially in the case of cold-drawn PET, where a large indentation anisotropy value is found. This is a consequence of the three-dimensional tensorial character of the microhardness [137]. The average hardness value for the isotropic material follows [151]:

$$\langle H \rangle = 2/3H_\perp + 1/3H_{chain} \tag{14}$$

where H_{chain} is the hardness value measured when the load is applied in the direction of the molecular axis. Since $H_{chain} > H_\perp$, then $\langle H \rangle$ is always larger than $H_\perp$.

6.2. Appearance of a phase of intermediate order

Starting from cold-drawn PET, a gradual increase of the degree of order can be achieved by means of annealing [152]. Bonart was the first researcher to observe the structural transformation taking place upon mechanical drawing of PET, from a totally amorphous into a nematic- and, finally, to a smectic-like state [153]. Furthermore Yeh and Geil showed, using electron microscopy, that glassy PET is composed of spherical-like structures in which the molecules exhibit a "paracrystalline" order [154]. The mechanism of transformation from the glassy nematic-like state to the smectic-like phase, and finally into the triclinic structure upon annealing has been the subject of a number of investigations [155–158]. These studies suggest that the smectic-like phase acts as a precursor for crystallization. An oriented mesophase has also been observed during the uniaxial deformation of PET above its glass transition temperature (hot drawing) [159]. Strain-induced crystallization of hot-drawn PET was found to occur mainly in the mesophase region,

in a similar manner as was previously suggested for cold-drawn PET.

The appearance of a smectic-like phase in cold-drawn PET upon annealing can be detected by means of WAXS. Fig. 17 illustrates the room temperature WAXS patterns of a cold-drawn PET sample annealed at different temperatures. The weak but well-defined reflection appearing in the meridian after annealing at a temperature, T_a, of 60 °C is associated to the appearance of a smectic-like phase. The intensity of this reflection increases for $T_a = 70$ °C and diminishes upon heating at higher temperatures ($T_a = 80$ °C), where the first crystals appear (note the 010 and 0$\bar{1}$1 reflections slightly away from the equator). Above 90 °C, only the triclinic structure can be detected. Indentation techniques have been shown to provide additional information on the smectic-like phase of oriented PET [132,155,160]. Fig. 18 offers a summary of the main results concerning the structure formation in glassy PET drawn at $\lambda \sim 4$ and further annealed at T_a, as revealed by microhardness. As mentioned above, the $H_\perp$ values are related to the plastic deformation mode of the lamellar stacks within the fibrous structure and one can distinguish four regions of hardness behaviour which correlate to the various structures appearing (see Fig. 18):

(a) At $T_a \leq 50$ °C: as we have seen in the foregoing, cold drawing of glassy PET induces preferential alignment of the chain axis along the draw direction. The orientational order exhibited can be described by a nematic-like state. Molecules are aligned roughly parallel to the draw direction and the lateral position of each benzene ring deviates with respect to the neighbouring molecules.

(b) At 50 °C $< T_a < 80$ °C: the hardness slightly varies with T_a: here the smectic-like phase appears, as revealed by a sharp WAXS meridional reflection [155]. Neighbouring molecular segments tend to laterally match at temperatures below T_g. The benzene rings are arranged on planes perpendicular to the draw direction.

(c) At 80 °C $< T_a < 90$ °C: the hardness increase above 70 °C can be considered as owing to an enhancement of molecular motion facilitated beyond T_g. The step variation of $H_\perp$ with T_a at 80 °C and above is associated with the development of a triclinic structure while the smectic domains start disappearing.

(d) At $T_a > 90$ °C: the smectic phase has completely disappeared and a three-dimensional crystalline order develops as revealed by small angle X-ray scattering (SAXS) and WAXS. The further $H_\perp$ increase above 100 °C can be related to the structural changes occurring in the fibrils [155].

Table 3
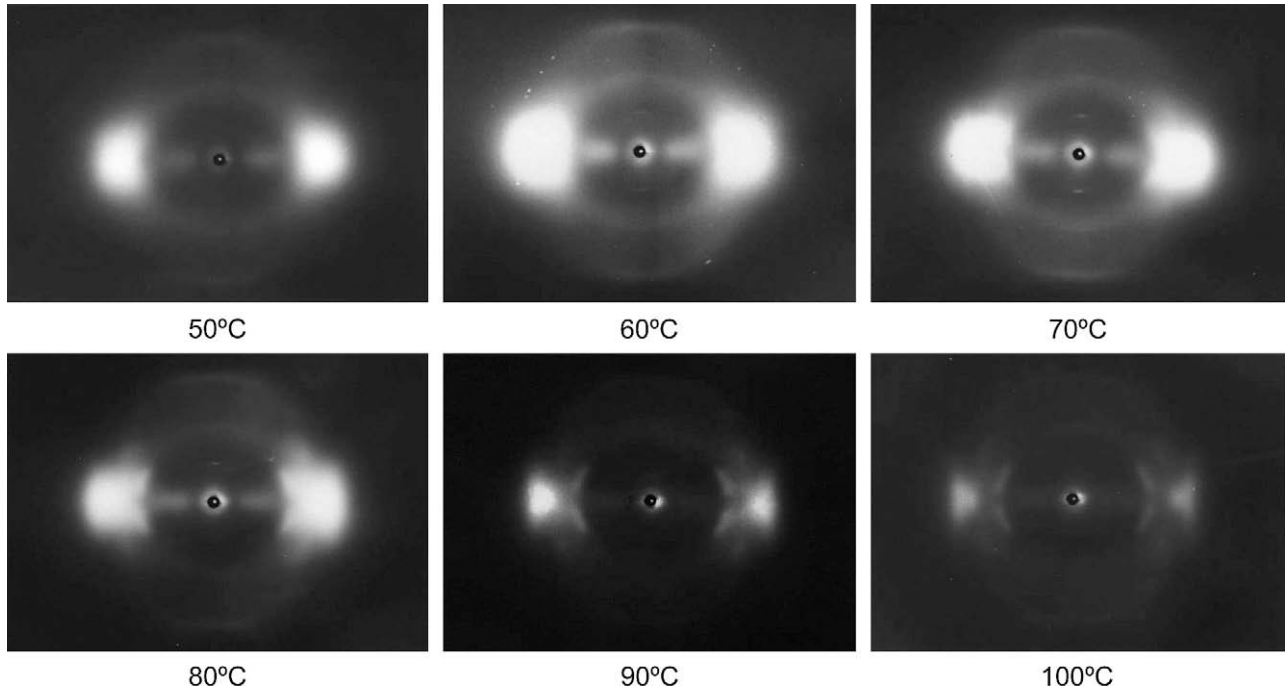Microhardness values measured in the direction perpendicular and parallel to drawing, $H_\perp$ and $H_\parallel$ respectively, for PET [33] and PMMA [150]. The corresponding indentation anisotropy values, ΔH, calculated using Eq. (13), are included. Microhardness values for isotropic PET [64,93,179] and PMMA [150], $\langle H \rangle$, are also shown.

Material	$H_\perp$ [MPa]	$H_\parallel$ [MPa]	ΔH	$\langle H \rangle$ [MPa]
Cold-drawn PET	65	120	0.46	
Hot-drawn PET	143	147	0	
Isotropic PET				110–150
Hot-drawn PMMA	162	194	0.17	
Isotropic PMMA				176

Fig. 17. WAXS patterns of cold-drawn PET at room temperature after annealing during 10 s at various temperatures. Reprinted from Polymer, Asano T, Baltá-Calleja FJ, Flores A, Tanigaki M, Mina MF, Sawatari C, Itagaki H, Takahashi H, Hatta I, Crystallization of oriented amorphous poly(ethylene terephthalate) as revealed by X-ray diffraction and microhardness, 40(23), 6475–84. Copyright (1999), with permission from Elsevier.

Summarizing the above analysis of hardness data, most interesting is the fact that one can detect the smectic phase by means of microindentation hardness measurements. In addition, the study also confirms that the micromechanical properties of the glass, the smectic-like and the crystalline phases are different.

Finally, Fig. 18 (inset) also illustrates the variation of the indentation anisotropy as a function of T_a. Results show that the indentation anisotropy first remains constant up to $T \sim 75\,°C$. It is only above T_g that ΔH decreases rapidly with increasing T up to $250\,°C$. This conspicuous decrease is most probably associated to the fact that the molecules within the amorphous layers relax and hence, the elastic recovery in the chain direction decreases. It is also

to be noted that X-ray measurements reveal that there is an inclination of the lamellae when the first crystals appear [33,155,160]. This inclination decreases as the annealing temperature rises. This would also facilitate the amorphous molecules connecting crystals to relax to less extended conformations, and hence, the elastic response will decrease. It is interesting to note that indentation anisotropy still remains preserved near the melting point.

6.3. Creep properties

In accordance with the concepts discussed in Section 4.3, creep can be defined as the time-dependent change in strain following a step change in stress [1]. Flores et al. [132] have investigated the creep behaviour and elastic properties of cold-drawn PET films, annealed in the range 60–240 °C by means of microindentation testing. This study demonstrates that the creep behaviour (visco-plastic flow) of the oriented material is intimately correlated to the nanostructural changes occurring upon annealing. Indeed, Fig. 19 illustrates the variation of the creep constant k, derived from Eq. (10), as a function of the crystalline lamellar thickness values. The periodicity of the meridional reflection associated with the smectic phase has been also included in Fig. 19 (1.07 nm). The rate of creep of the glassy material is shown to diminish with the appearance of smectic domains, which confers to the material a higher structural order. This result is in agreement with previous microindentation hardness studies on amorphous PET films with different degrees of internal order [64]. In addition, Fig. 19 shows that a further decrease in the creep constant is observed first with the development of triclinic crystalline order, and thereafter with the increase of crystal lamellar thickness [132]. The k values steeply decrease with increasing crystal thickness for small l_c values while a levelling-off occurs for large crystal thickness values. Previous studies on chain-extended polyethylene, chain-folded polyethylene, and a series of paraffins report similar creep dependence with crystal thickness [91].

In summary, the study of the visco-plastic properties of annealed cold-drawn PET films reveals that the glassy unannealed
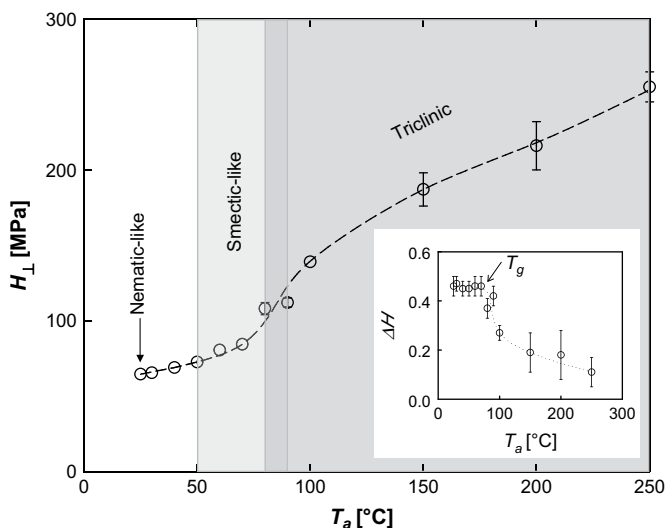
Fig. 18. Variation of $H_\perp$ as a function of annealing temperature for cold-drawn PET. The inset shows the indentation anisotropy values for the same annealed samples. Replotted from Ref. [33].
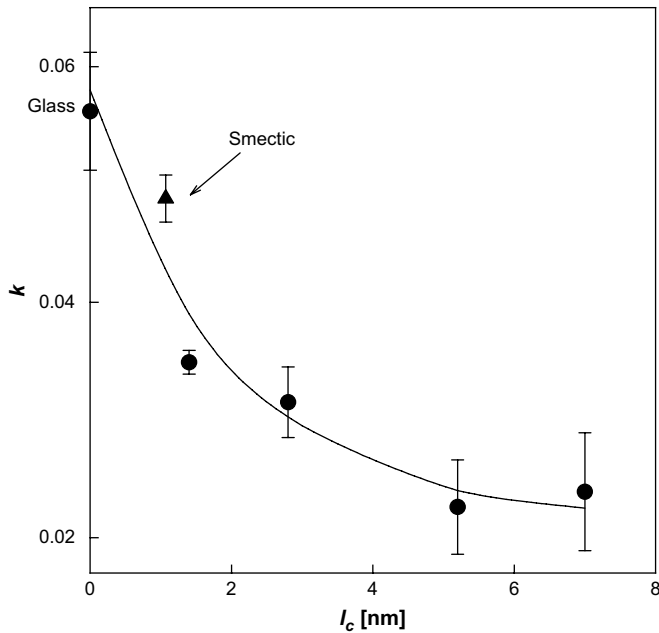
Fig. 19. Variation of the creep constant k as a function of crystal thickness l_c for cold-drawn PET samples annealed at different temperatures. Solid triangle corresponds to the periodicity of the meridional reflection associated to the smectic phase. Reprinted with permission from [Flores A, Baltá-Calleja FJ, Asano T. J Appl Phys 2001;90(12):6006–10]. Copyright (2001), American Institute of Physics.

Fig. 20. Typical load–displacement curve for a silk membrane after a loading and unloading cycle. Reprinted from Polymer, Puente Orench I, Putthanarat S, Baltá-Calleja FJ, Eby RK, Stone M, Ultra-microindentation at the surface of silk membranes, 45(6), 2041–4. Copyright (2004), with permission from Elsevier.

material flows at the highest rate. The rate of creep is found to diminish with increasing thickness of the crystalline lamellae. The creep constant value for the smectic phase lies in between that corresponding to the glassy material and those associated to the triclinic structure. This finding suggests that the visco-plastic flow of cold-drawn PET diminishes with increasing structural order of the material and supports the concept of the smectic-like phase being a precursor state of crystallization.

7. Depth-sensing measurements: state-of-the art and perspectives

As mentioned in Section 1, depth-sensing measurements of hardness are becoming standard in the last few years. This is due to the development of highly accurate instruments, which provide more information than the traditional optical measurements. The technique consists in continuously measuring the load applied by the indenter as a function of the penetration depth. The first depth-sensing instruments were built in the early 1980s [161]. Much of the effort in the following years was directed towards the establishment of a standard procedure to analyze depth-sensing data. The most successful ones were those developed by Doerner and Nix [22] and Oliver and Pharr (O–P) [24]. Both methods assume that deformation on loading is both elastic and plastic, while on unloading only the elastic displacements recover. Values of hardness and elastic modulus can be obtained from the initial unloading data. Fig. 20 shows an example of load (and unload)–displacement curves for a silk membrane tested with a Vickers diamond at 10 mN maximum indentation load P_{max} [162]. Hardness can be derived according to [22,24]:

$$H = P_{max}/A \tag{15}$$

where A is the projected contact area of the indenter under load. This H value may deviate from the one obtained through the optical measurement of the residual impression if the elastic recovery during unloading is significant.
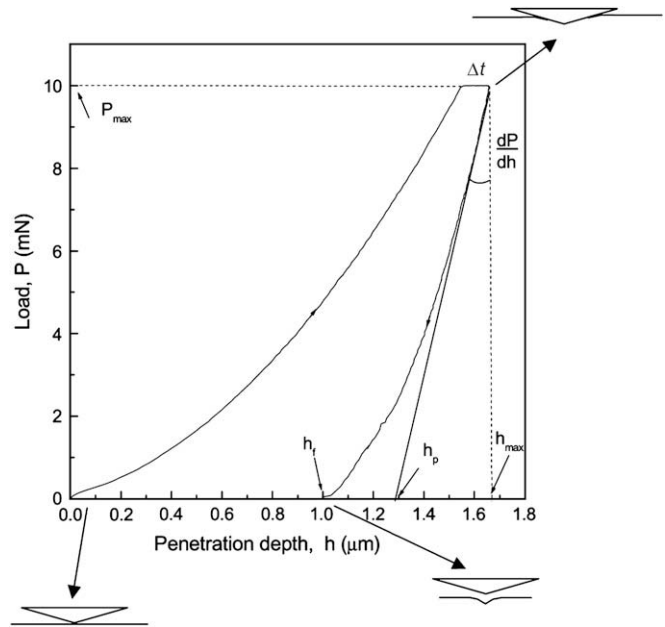
The effective elastic modulus E_{eff} can be calculated from the initial slope dP/dh of the unloading curve, which is also known as contact stiffness S:

$$E_{eff} = 1/\beta(\pi/A)^{1/2}S/2 \tag{16}$$

where β is a dimensionless parameter [24,25]. Eq. (16) applies to a good number of axisymmetric indenter geometries.

Finally, the elastic modulus E of the material can be obtained from:

$$1/E_{eff} = \left(1 - \nu^2\right)/E + \left(1 - \nu_i^2\right)/E_i \tag{17}$$

ν being the Poisson's ratio of the material and ν_i and E_i corresponding to the elastic properties of the indenter.

In the case of polymer materials, due to the fact that $E_i \gg E$, Eq. (17) can be simply given as:

$$E = E_{eff}\left(1 - \nu^2\right) \tag{18}$$

The analysis of the O–P method is essentially an extension of the one by Doerner and Nix. The latter assumes a flat-punch approximation for the initial portion of the unloading curve, which implies a linear behaviour (constant contact area). In contrast, O–P accounts for the curvature frequently observed for the unloading data, as a consequence of the continuous change of the contact area as the indenter is withdrawn. In the last decade, the O–P method has been widely adopted to characterize the mechanical behaviour of materials from depth-sensing instrumentation [25].

Early work on polymers using loads in the lower limit of conventional microhardness tests [163,164] reported a good correlation between hardness values obtained optically and by depth sensing, after analyzing the latter data according to the O–P method. For instance, the elastic modulus values of thermally treated *Bombyx mori* silk membranes, derived from hardness tests (Fig. 20), yield similar results to those obtained by other methods for silk membranes and fibres. It is noteworthy that H depends on the nanofibril size of the different silk samples and the values found around 400 MPa are among the

highest ones in all the range of polymers studied [162]. It was soon realized, however, that the determination of hardness for polymers by means of the Oliver and Pharr procedure could yield very large errors. The main source of error is that the O–P method does not take into account time-dependent deformation mechanisms such as creep or viscoelasticity, which are extremely important in polymer materials. In other words, to characterize the mechanical properties it is necessary to envisage a constitutive model which takes into account not only time-independent elasto-plastic but also visco-elastic–visco-plastic deformations [165]. Several approaches have been proposed in recent years which offer the possibility of accurately extracting hardness and elastic modulus of polymer materials from the loading and unloading cycles [19,130,165–167].

Latest developments of the nanoindentation technique include the possibility of changing "in situ" the temperature of the sample [168,169]. In this way, for example, the nanomechanical properties of PET films in a temperature range of 60–110 °C have been investigated as a function of crystallinity and processing history [169]. However, what is conceiving more expectations from an instrumental point of view is the possibility of superposing a small modulated load to the usual indentation load, or applying an oscillation to the position of the sample [170], to calculate modulus and hardness continuously throughout the complete loading history. The reason is that the contact stiffness S can be measured as a function of depth and not just at the point of unloading. In this way, the time constant of the experiment is much smaller than that of the non-modulated method and, in addition, measurements can be performed at exceedingly small penetration depths. Furthermore, other important advantage of dynamic methods lies on the possibility of characterizing the viscoelastic properties of the materials by means of the storage and loss moduli, E' and E'', and the loss tangent [171]. Thus, information on the glass transition temperature, mechanical relaxation and activation energy for the relaxation processes can be obtained. So far, one of the limitations of depth-sensing instrumentation is the small range of frequencies of the modulated load (usually within 1–300 Hz). However, the time–temperature superposition can be accomplished on the frequency domain to extend the range of frequencies [172].

To extract E' and E'' from depth-sensing data, let us define the oscillating force superimposed upon the indenter load as $P(t) = P_0 e^{i\omega t}$. The displacement produced can be expressed as $h(t) = h_0 e^{i(\omega t - \phi)}$, where ϕ represents the phase difference between them. By assuming a certain mechanical model for the dynamic indentation, an expression of the oscillating force $P(t)$ in terms of the characteristic parameters of the instrument, together with those depending on the materials and the conditions at the contacting surfaces, can be obtained [173–175]. The contact stiffness S can be calculated from the displacement signal or from the phase difference ϕ. In the end, taking into account the definition of the complex modulus of a viscoelastic material, $E = E' + iE''$ and by implementing the elastic solution for the elastic modulus from nanoindentation and the elastic–viscoelastic correspondence principle, both the storage modulus E' and the loss modulus E'' of a polymer can be determined according to [175]:

$$E'_{\text{eff}} = 1/(2\beta)(\pi/A)^{1/2} S \tag{19}$$

$$E''_{\text{eff}} = \omega C_s/(2\beta)(\pi/A)^{1/2} \tag{20}$$

where C_s is the contact damping.

Dynamic nanoindentation measurements have been conducted in different polymer systems including glassy polymers PMMA, PS, PC [19,170], polyolefins [173,175,176], or a series of polymers with different crosslink densities [177]. In general, a good agreement has been found between the complex modulus obtained by nanoindentation and conventional dynamic mechanical analysis (DMA) tests, although the reliability of the former method strongly depends on the calibration of the characteristic parameters of the instrument used [170].

As a final point, it is worth mentioning that atomic force microscopy (AFM) has proven to be a useful depth-sensing instrument for soft samples, mainly polymers and biological materials. In spite of the common idea that AFM measurements can only provide semiquantitative results, new methods which include the determination of several instrumental and calibration parameters permit to accurately study the contact mechanics and the mechanical behaviour of polymers during indentation on the nanometer scale [178].

8. Conclusions

The development of new advanced polymeric materials for a variety of applications has emphasized research into the understanding of nanostructure, morphology and local deformation mechanisms. Microindentation hardness appears to be a bridging property between nanostructure, morphology and mechanical properties offering direct information about the micromechanical processes occurring at microscopic and nanoscopic level: the so-called field of micromechanics. Hardness within this context is defined as a measure of the resistance of a material to shear stresses under local volume (μm to nm range) compression. This article shows that indentation hardness is a useful technique for the understanding of the development of order which proceeds from the glassy state to more ordered structures in polymers.

Early developments in these areas showed that it is possible to detect accurately the glass transition temperature of glassy polymers by measurement of microhardness as a function of temperature. Furthermore, it is the morphology of the polymer that will ultimately determine the micromechanical properties. Indeed, it has been recently shown that the microhardness behaviour of glassy star block copolymers and PS blends strongly depends on the phase morphology. For example, a higher hardness rate increase is observed when the morphology changes from stacks of alternating lamellae to that of the PS matrix.

Nanocomposites are a subject of wide interest. It has been shown that the structure of the filler strongly influences the microhardness of glassy polymers (PC)–carbon black composites. Smaller filler aggregates are found to induce a clear enhancement of microhardness due to a more homogenous dispersion of the microadditive.

Microhardness can readily detect the nanostructural development from the glass during crystallization, providing valuable information on this process. Microindentation studies in physically confined systems, such as PET/PC multilayer films, show lower final limiting hardness values than in the non-confined case. This is consequence of the dramatic crystallinity decrease below the μm range.

Crystallinity and crystal thickness are shown to be the two leading parameters defining the final micromechanical properties of the polymer material. Creep properties are also reviewed and discussed in terms of variations in the internal degree of order, orientation, filler reinforcement, temperature and branching of a diversity of polymer materials.

The microhardness of an ethylene based material having nearly zero crystallinity has been recently reported. Ethylene-*co*-octene copolymers exhibit a large deviation from the microhardness additivity law of the individual phases (crystalline and amorphous). Deviations from the additivity law predictions also characterize the micromechanical behaviour of other polymer materials with low degree of crystallinity and $T_g < T_{\text{room}}$, such as a series of block

copolyester amides. A different mode of deformation is envisaged for these polymer materials with marked elastomeric character with respect to those with $T_g > T_{room}$. In the former, crystallites are dispersed in a viscous amorphous material in a minor amount and 'slide' within the amorphous matrix upon indentation.

The effect of molecular orientation in stretched glassy polymer materials has been also reviewed as it plays a critical role in the mechanical properties of the precursors of crystallization. The microhardness behaviour of annealed cold-drawn PET is correlated to the developing morphologies. In addition, the creep behaviour of cold-drawn PET annealed above T_g is also correlated to the nanostructure of the oriented material.

In summary, the selected examples in this article emphasize attractive applications of the microindentation method to the study of the mechanical properties of polymer surfaces. It is specific in suggesting further microhardness morphology correlations of flexible and rigid glassy polymers, blends, composites, and non-crystallizable glasses. In addition, depth-sensing techniques have been introduced and recent methods to derive the visco-elasto-plastic properties at the near-surface region of polymers, through nanoindentation, have been outlined. The application of a small oscillation load superimposed to the usual load, or a small modulated displacement of the sample, offers new possibilities to determine the dynamic mechanical properties and it constitutes a most challenging technique for the near future.

Acknowledgements

References

[1] Ward IM, Sweeney J. An introduction to the mechanical properties of solid polymers. Chichester: John Wiley; 2004.
[2] Shonaike GO, Advani SG. Advanced polymer materials. Boca Raton (Florida): CRC Press; 2003.
[3] Shalaby SW, Burg KJL. Absorbable and biodegradable polymers. Boca Raton (Florida): CRC Press; 2004.
[4] Meyers MA, Ritchie RO, Rarikaya M, editors. Nano and microstructural design of advanced materials. Amsterdam: Elsevier; 2006.
[5] Michler GH, Baltá-Calleja FJ, editors. Mechanical properties of polymers based on nanostructure and morphology. Boca Raton (Florida): Taylor and Francis; 2005.
[6] Baltá-Calleja FJ, Fakirov S. The microhardness of polymers. Cambridge: Cambridge University Press; 2000.
[7] Baltá-Calleja FJ, Fakirov S. Trends Polym Sci 1997;5(8):246–9.
[8] Baltá-Calleja FJ, Flores A, Ania F. In: Michler GH, Baltá-Calleja FJ, editors. Mechanical properties of polymers based on nanostructure and morphology. Boca Raton (Florida): Taylor and Francis; 2005 [chapter 8].
[9] Marsh DM. Proc R Soc London Ser A 1964;279:420–35.
[10] Hirst W, Howse MGJW. Proc R Soc London Ser A 1969;311:429–44.
[11] Johnson KL. Contact mechanics. Cambridge: Cambridge University Press; 1985. p. 171.
[12] Studman CJ, Moore MA, Jones SE. J Phys D Appl Phys 1977;10:949–56.
[13] Perrott CM. Wear 1977;45:293–309.
[14] Hill R. Proc R Soc London Ser A 1992;436:617–30.
[15] Cheng Y-T, Cheng C-M. Mater Sci Eng 2004;44:91–149.
[16] Kermouche G, Loubet JL, Bergheau JM. C R Mech 2005;333:389–95.
[17] Rikards R, Flores A, Ania F, Kushnevski V, Baltá-Calleja FJ. Comput Mater Sci 1998;11:233–44.
[18] Bucaille JL, Felder E, Hochstetter G. J Mater Sci 2002;37(18):3999–4011.
[19] Kermouche G, Loubet JL, Bergheau JM. Mech Mater 2008;40:271–83.
[20] Tabor D. The hardness of metals. Oxford: Oxford University Press; 2000. Oxford classic series.
[21] Flores A, Baltá-Calleja FJ, Attenburrow GE, Bassett DC. Polymer 2000;41:5431–5.
[22] Doerner MF, Nix WD. J Mater Res 1986;1(4):601–9.
[23] Pharr GM, Oliver WC, Brotzen FR. J Mater Res 1992;7(3):613–7.
[24] Oliver WC, Pharr GM. J Mater Res 1992;7(6):1564–83.
[25] Oliver WC, Pharr GM. J Mater Res 2004;19(1):3–20.
[26] Baltá-Calleja FJ, Flores A, Michler GH. J Appl Polym Sci 2004;93(4):1951–6.
[27] Puente Orench I, Ania F, Baer E, Hiltner A, Bernal T, Baltá-Calleja FJ. Philos Mag 2004;84(18):1841–52.
[28] Baltá-Calleja FJ, Cagiao ME, Adhikari R, Michler GH. Polymer 2004;45(1):247–54.
[29] Henning S, Michler GH, Ania F, Baltá-Calleja FJ. Colloid Polym Sci 2005;283(5):486–95.
[30] Flores A, Pieruccini M, Stribeck N, Funari SS, Bosch E, Baltá-Calleja FJ. Polymer 2005;46(22):9404–10.
[31] Ania F, Broza G, Mina MF, Schulte K, Roslaniec Z, Baltá-Calleja FJ. Compos Interfaces 2006;13(1):33–45.
[32] Flores A, Mathot VBF, Michler GH, Adhikari R, Baltá-Calleja FJ. Polymer 2006;47(15):5602–9.
[33] Uchiyama T, Suyama M, Alam MM, Asano T, Henning S, Flores A, et al. Polymer 2007;48(2):542–55.
[34] Shahdad SA, McCabe JF, Bull S, Rusby S, Wassell RW. Dent Mater 2007;23(9):1079–85.
[35] Bembey AK, Oyen ML, Bushby AJ, Boyde A. Philos Mag 2006;86(33–35):5691–703.
[36] Godara A, Raabe D, Green S. Acta Biomater 2007;3(2):209–20.
[37] Liu Y, Wang M. J Appl Polym Sci 2007;106(4):2780–90.
[38] Vaziri A, Lee H, Mofrad MRK. J Mater Res 2006;21(8):2126–35.
[39] Kaufman JD, Miller GJ, Morgan EF, Klapperich CM. J Mater Res 2008;23(5):1472–81.
[40] Lu HB, Huang G, Wang B, Mamedov A, Gupta S. Thin Solid Films 2006;500(1–2):197–202.
[41] Owens FJ. J Mater Chem 2006;16(5):505–8.
[42] Chiu WM, Chang YA, Kuo HY, Lin MH, Wen HC. J Appl Polym Sci 2008;108(5):3024–30.
[43] Liu TX, Phang IY, Shen L, Chow SY, Zhang WD. Macromolecules 2004;37(19):7214–22.
[44] Chavarria F, Paul DR. Polymer 2006;47(22):7760–73.
[45] Shen L, Phang IY, Liu TX, Zeng KY. Polymer 2004;45(24):8221–9.
[46] Wornyo E, Gall K, Yang FZ, King W. Polymer 2007;48(11):3213–25.
[47] Chen CH, Sun YY. J Appl Polym Sci 2006;101(3):1826–32.
[48] Flores A, Pietkiewicz D, Stribeck N, Roslaniec Z, Baltá-Calleja FJ. Macromolecules 2001;34(23):8094–100.
[49] Bartolomeo P, Irigoyen M, Aragón E, Frizzi MA, Perrin FX. Polym Degrad Stab 2001;72(1):63–8.
[50] Maxwell AS. Polym Eng Sci 2008;48(2):381–5.
[51] Rodríguez RJ, Medrano A, García JA, Fuentes GG, Martínez R, Puértolas JA. Surf Coat Technol 2007;201(19–20):8146–9.
[52] Valenza A, Visco AM, Torrisi L, Campo N. Polymer 2004;45(5):1707–15.
[53] Shah N, Singh D, Shah S, Qureshi A, Singh NL, Singh KP. Bull Mater Sci 2007;30(5):477–80.
[54] Mishra AK, Agrawal P, Bajpai R. J Appl Polym Sci 2004;92(5):3107–11.
[55] López-Quintana S, Rosales C, Gobernado-Mitre I, Merino JC, Pastor JM. Polymer 2004;45(23):8041–50.
[56] Rueda DR, Varkalis A, Viksne A, Baltá-Calleja FJ, Zachmann HG. J Polym Sci Part B Polym Phys 1995;33:1653–61.
[57] Kusy RP, Whitley JQ, Kalachandra S. Polymer 2001;42(6):2585–95.
[58] Katare R, Bajpai R, Datt SC. Polym Test 1994;13(2):107–12.
[59] Crist B. Plastic deformation of polymers. In: Thomas EL, editor. Materials science and technology, vol. 12. Weinheim: VCH; 1993. p. 427–69.
[60] Gedde UW. Polymer physics. London: Chapman and Hall; 1995. p. 78.
[61] Fakirov S, Baltá-Calleja FJ, Krumova M. J Polym Sci Part B Polym Phys 1999;37:1413–9.
[62] Baltá-Calleja FJ, Privalko EG, Fainleib AM, Shantalii TA, Privalko VP. J Macromol Sci Phys 2000;B39(2):131–41.
[63] Scrivani T, Benavente R, Pérez E, Pereña JM. Macromol Chem Phys 2001;202:2547–53.
[64] Rueda DR, García Gutiérrez MC, Baltá-Calleja FJ, Piccarolo S. Int J Polym Mater 2002;51:897–908.
[65] Baltá-Calleja FJ, García Gutiérrez MC, Rueda DR, Piccarolo S. Polymer 2000;41(11):4143–8.
[66] Piccarolo S, Saiu M, Brucato V, Titomanlio G. J Appl Polym Sci 1992;46(4):625–34.
[67] Piccarolo S. J Macromol Sci Phys 1992;B31(4):501–11.
[68] Volynskii AL, Efimov AV, Bakeev NF. Polym Sci Ser C 2007;49(4):301–20.
[69] Flores A, Cagiao ME, Ezquerra TA, Baltá-Calleja FJ. J Appl Polym Sci 2001;79(1):90–5.
[70] Holden G. Understanding thermoplastic elastomers. Munich: Carl Hanser Verlag; 2000.
[71] Hamley IW. The physics of block copolymers. Oxford: Oxford Science Publications; 1998.
[72] Michler GH, Baltá-Calleja FJ, Puente I, Cagiao ME, Knoll K, Henning S, et al. J Appl Polym Sci 2003;90:1670–7.
[73] Martínez Salazar J, Canalda Cámara JC, Baltá-Calleja FJ. J Mater Sci 1991;26:2579–82.
[74] Baltá-Calleja FJ, Santa Cruz C, Chen D, Zachmann HG. Polymer 1991;32(12):2252–7.
[75] Giri L, Roslaniec Z, Ezquerra TA, Baltá-Calleja FJ. J Macromol Sci Phys 1997;B36(3):335–43.
[76] Michler GH, Adhikari R, Lebek W, Goerlitz S, Weidish R, Knoll K. J Appl Polym Sci 2002;24:683–700.
[77] Dutta NK, Tripathy DK. J Appl Polym Sci 1992;44:1635–48.
[78] Khaled MA, Hassan EA, Elwy A, Metwally EE. Mater Lett 1994;19:325–8.
[79] Debnath SC, Mandal SK, Basu DK. J Appl Polym Sci 1995;57:555–62.
[80] Huang JC, Huang HL. J Polym Eng 1997;17:213–29.

[81] Hamza SS. Polym Test 1998;17:131–7.
[82] Huang JC, Chaung SF, Su TY, Grossman SJ. J Polym Eng 1999;19:39–52.
[83] Koszkul J. J Polym Eng 1998;18:249–62.
[84] Pinto G, López-González C, Jiménez-Martín A. Polym Compos 1999; 20(6):804–8.
[85] Ezquerra TA, Martínez Salazar J, Baltá-Calleja FJ. J Mater Sci Lett 1986;5:1065–6.
[86] Jiang X, Bin Y, Matsuo M. Polymer 2005;46:7418–24.
[87] Meincke O, Kaempfer D, Weickmann H, Friedrich C, Vathauer M, Warth H. Polymer 2004;45:739–48.
[88] Flores A, Ania F, Baltá-Calleja FJ. Polymer 1997;38(21):5447–53.
[89] Ania F, Martínez Salazar J, Baltá-Calleja FJ. J Mater Sci 1989;24:2934–8.
[90] Kajaks J, Flores A, García Gutiérrez MC, Rueda DR, Baltá-Calleja FJ. Polymer 2000;41(21):7769–72.
[91] Baltá-Calleja FJ, Flores A, Ania F, Bassett DC. J Mater Sci 2000;35:1315–9.
[92] Puente Orench I. Ph.D. thesis, Universidad Autónoma de Madrid; 2006.
[93] Baltá-Calleja FJ, Santa Cruz C, Asano T. J Polym Sci Part B Polym Phys 1993;31:557–65.
[94] Pastor JM, González A, De Saja JA. J Appl Polym Sci 1989;38:2283–8.
[95] Connor MT, García Gutiérrez MC, Rueda DR, Baltá-Calleja FJ. J Mater Sci 1997;32:5615–20.
[96] Santa Cruz C, Baltá-Calleja FJ, Zachmann HG, Stribeck N, Asano T. J Polym Sci Part B Polym Phys 1991;29:819–24.
[97] Cagiao ME, Connor M, Baltá-Calleja FJ, Seferis JC. Polym J 1999;31(9):739–46.
[98] Rueda DR, Viksne A, Malers L, Baltá-Calleja FJ, Zachmann HG. Macromol Chem Phys 1994;195:3869–76.
[99] Baltá-Calleja FJ. Structure–microhardness correlation of polymers and blends. In: Cunha AM, Fakirov S, editors. Structure development during polymer processing. NATO science series, vol. 370E. Dordrecht: Kluwer Academic Publishers; 2000. p. 145–62.
[100] Flores A, Aurrekoetxea J, Gensler R, Kausch HH, Baltá-Calleja FJ. Colloid Polym Sci 1998;276:786–93.
[101] Bayer RK, Baltá-Calleja FJ, Kilian HG. Colloid Polym Sci 1997;275:432–9.
[102] Flores A, Baltá-Calleja FJ, Bassett DC. J Polym Sci Part B Polym Phys 1999;37:3151–8.
[103] Martínez-Salazar J, García Tijero JM, Baltá-Calleja FJ. J Mater Sci 1988;23:862–6.
[104] Boneva D, Baltá-Calleja FJ, Fakirov S, Apostolov AA, Krumova M. J Appl Polym Sci 1998;69:2271–6.
[105] Fakirov S, Boneva D, Baltá-Calleja FJ, Krumova M, Apostolov AA. J Mater Sci Lett 1998;17:453–7.
[106] Baltá-Calleja FJ, Baranowska J, Rueda DR, Bayer RK. J Mater Sci 1993;28:6074–80.
[107] Vanderdonckt C, Krumova M, Baltá-Calleja FJ, Zachmann HG, Fakirov S. Colloid Polym Sci 1998;276:138–43.
[108] García Gutiérrez MC, Rueda DR, Baltá-Calleja FJ, Stribeck N, Bayer RK. Polymer 2003;44(2):451–5.
[109] Deslandes Y, Alva Rosa E, Brisse F, Meneghini T. J Mater Sci 1991;26:2769–77.
[110] Parlevliet PP, van der Werf WAW, Bersee HEN, Beukers A. Compos Sci Technol 2008;68(3–4):896–907.
[111] Palathai T, Tharajak J, Sombatsompop N. Mater Sci Eng A 2008;485(1–2):66–73.
[112] Baltá-Calleja FJ, Rueda DR, Michler GH, Naumann IJ. Macromol Sci Phys 1998;37:411–9.
[113] Baer E, Hiltner A, Morgan R. Phys Today 1992;October:60–7.
[114] Loo YL, Register RA, Ryan AJ, Dee GT. Macromolecules 2001;34:8968–77.
[115] Jin Y, Rogunova M, Hiltner A, Baer E, Nowacki AR, Galeski A, et al. J Polym Sci Part B Polym Phys 2004;42(18):3380–96.
[116] Liu RRYF, Hiltner A, Baer E. Macromol Rapid Commun 2003;24:943–8.
[117] Bernal-Lara TE, Ranade A, Hiltner A, Baer E. In: Michler GH, Baltá-Calleja FJ, editors. Mechanical properties of polymers based on nanostructure and morphology. Boca Raton: CRC, Taylor & Francis; 2005. p. 629–81.
[118] Kazmierczak T, Song H, Hiltner A, Baer E. Macromol Rapid Commun 2007;28:2210–6.
[119] Baltá-Calleja FJ, Ania F, Puente Orench I, Baer E, Hiltner A, Bernal T, et al. Prog Colloid Polym Sci 2005;130:140–8.
[120] Baltá-Calleja FJ. Colloid Polym Sci 1976;254:258–66.
[121] Baltá-Calleja FJ, Kilian HG. Colloid Polym Sci 1985;263:697–707.
[122] Baltá-Calleja FJ, Santa Cruz C. Acta Polym 1996;47:303–9.
[123] Azzurri F, Flores A, Alfonso GC, Sics I, Hsiao BS, Baltá-Calleja FJ. Polymer 2003;44(5):1641–5.
[124] Ion RH, Pollock HM, Roques-Carmes C. J Mater Sci 1990;25:1444–54.
[125] Van Landingham MR, Chang NK, Drzal PL, White CC, Chang SH. J Polym Sci Part B Polym Phys 2005;43:1794–811.
[126] Tweedie CA, Van Vliet KJ. J Mater Res 2006;21(6):1576–89.
[127] Beake B. J Phys D Appl Phys 2006;39:4478–85.
[128] Beake BD, Bell GA, Brostow W, Chonkaew W. Polym Int 2007;56:773–8.
[129] Bell GA, Bielinski DM, Beake BD. J Appl Polym Sci 2008;107:577–82.
[130] Yang S, Zhang YW, Zeng K. J Appl Phys 2004;95(7):3655–66.
[131] Minkova L, Peneva Y. Polymer 2003;44(21):6483–6.
[132] Flores A, Baltá-Calleja FJ, Asano T. J Appl Phys 2001;90(12):6006–10.
[133] Mina MF, Ania F, Huy TA, Michler GH, Baltá-Calleja FJ. J Macromol Sci Phys 2005;43(5):947–61.
[134] Flores A, Bayer RK, Krawietz K, Baltá-Calleja FJ. J Macromol Sci Phys 2000;39:749–59.
[135] Berdjane K, Berdjane Z, Rueda DR, Bénachour D, Baltá-Calleja FJ. J Appl Polym Sci 2003;89:2046–50.
[136] Perrin FX, Nguyen V, Vernet JL. Polymer 2002;43(23):6159–67.
[137] Baltá-Calleja FJ. Adv Polym Sci 1985;66:117–48.
[138] Baltá-Calleja FJ, Rueda DR, Porter RS, Mead WT. J Mater Sci 1980;15:765–72.
[139] Mulhearn TO, Tabor D. J Inst Met 1960;89:7–12.
[140] Gourrier A, García Gutiérrez MC, Riekel C. Macromolecules 2002;35:8072–7.
[141] Gourrier A, García-Gutiérrez MC, Riekel C. Macromolecules 2005;38:3838–44.
[142] Gourrier A, García-Gutiérrez MC, Riekel C. Philos Mag A 2006;86(33–35):5753–67.
[143] Palza H, López-Majada JM, Quijada R, Benavente R, Pérez E, Cerrada ML. Macromol Chem Phys 2005;206:1221–30.
[144] Arranz-Andrés J, Suárez I, Peña B, Benavente R, Pérez E, Cerrada ML. Macromol Chem Phys 2007;208:1510–21.
[145] Vanden Eynde S, Mathot VBF, Koch MHJ, Reynaers H. Polymer 2000; 41(13):4889–900.
[146] Fakirov S. J Mater Sci 2007;42(4):1131–48.
[147] Rueda DR, Bayer RK, Baltá-Calleja FJ, Zachmann HG. J Macromol Sci Phys 1989;B28(2):265–82.
[148] Göschel U. Polymer 1995;36(6):1157–65.
[149] Göschel U, Deutscher K, Abetz V. Polymer 1996;37(1):1–6.
[150] Mina MF, Ania F, Baltá-Calleja FJ, Asano T. J Appl Polym Sci 2004;91:205–10.
[151] Santa Cruz C, Baltá-Calleja FJ, Asano T, Ward IM. Philos Mag A 1993; 68(1):209–24.
[152] Asano T, Seto T. Polym J 1973;5(1):72–85.
[153] Bonart R. Kolloid Z Z Polym 1966;213(1–2):1–11.
[154] Yeh GSY, Geil PHJ. J Macromol Sci Phys 1967;B1:235–49.
[155] Asano T, Baltá-Calleja FJ, Flores A, Tanigaki M, Mina MF, Sawatari C, et al. Polymer 1999;40(23):6475–84.
[156] Nicholson TM, Davies GR, Ward IM. Polymer 1994;35(20):4259–62.
[157] Welsh GE, Blundell DJ, Windle AH. Macromolecules 1998;31:7562–5.
[158] Kawakami D, Ran S, Burger C, Fu B, Sics I, Chu B, et al. Macromolecules 2003;36:9275–80.
[159] Kawakami D, Hsiao BS, Ran S, Burger C, Fu B, Sics I, et al. Polymer 2004; 45(3):905–18.
[160] Asano T, Forhad Mina MD, Fujiwara Y. A survey of polymer crystallization by X-ray diffraction. Shizuoka: SKP Inc; 2006.
[161] Pethica JB, Hutchings R, Oliver WC. Philos Mag A 1983;48(4):593–606.
[162] Puente Orench I, Putthanarat S, Baltá-Calleja FJ, Eby RK, Stone M. Polymer 2004;45(6):2041–4.
[163] Flores A, Baltá-Calleja FJ. Philos Mag A 1998;78(6):1283–97.
[164] Briscoe BJ, Sebastian KS, Sinha SK. Philos Mag A 1996;74(5):1159–69.
[165] Zhang CY, Zhang YW, Zeng KY, Shen L. Philos Mag 2006;86(28):4487–506.
[166] Liu CK, Lee S, Sung LP, Nguyen T. J Appl Phys 2006;100:033503-1–033503-9.
[167] Oyen ML. Philos Mag 2006;86(33–35):5625–41.
[168] Juliano TF, Van Landingham MR, Tweedie CA, Vav Vliet KJ. Exp Mech 2007;47(1):99–105.
[169] Gray A, Beake BD. J Nanosci Nanotechnol 2007;7(7):2530–3.
[170] Shing SP, Smith JF, Singh RP. Exp Mech 2008;48:571–83.
[171] Syed Asif SA, Wahl KJ, Colton RJ. Rev Sci Instrum 1999;70:2408–13.
[172] Hayes SA, Goruppa AA, Jones FR. J Mater Res 2004;19(11):3298–306.
[173] Loubet JL, Oliver WC, Lucas BN. J Mater Res 2000;15(5):1195–8.
[174] Li X, Bhushan B. Mater Charact 2002;48:11–36.
[175] Odegard GM, Gates TS, Herring HM. Exp Mech 2005;45(2):130–6.
[176] Bouaita N, Bull SJ, Fernández Palacio J, White JR. Polym Eng Sci 2006; 46:1160–72.
[177] White CC, Vanlandingham MR, Drzal PL, Chang NK, Chang SH. J Polym Sci Part B Polym Phys 2005;43:1812–24.
[178] Tranchida D, Piccarolo S, Soliman M. Macromolecules 2006;39(13):4547–56.
[179] Lorenzo V, Pereña JM. J Appl Polym Sci 1990;39:1467–74.

Dr. Araceli Flores, Research Scientist – Institute for Structure of Matter, CSIC, Madrid. Dr. Flores was born in 1966. She studied Physics at the University Autónoma of Madrid (1984–1989) and received her Ph.D. at the same University in 1993. She initiated her post-doctoral studies at the University of Cambridge in the period 1994–1996. In 2003, she became Research Scientist in the Macromolecular Physics Department of the Institute for Structure of Matter (CSIC), Madrid. Dr. Flores has published more than 40 papers and a number of book chapters. She has also contributed to articles of general public interest. She has been involved in the organization of scientific events for students and chaired two sessions in respective international meetings. Dr. Flores is a founding member of the Spanish Association of Synchrotron Radiation Users (AUSE), and has a large experience as a user in Synchrotron Radiation Sources. Her research interest is the structure–properties' relationship in polymers, with particular emphasis on the mechanical properties at different scales.

Dr. Fernando Ania, Research Scientist – Institute for Structure of Matter, CSIC, Madrid. He studied Physics at the University Complutense of Madrid. In 1982 he received his Ph.D. at the same University. Later he obtained a Royal Society of London Postdoctoral Fellowship in the University of Leeds (UK). In 1983 he became CSIC fellow at the University of Paderborn (Germany) for two years. Postdoctoral studies were continued in 1985 at the University of Ulm (Germany). In 1986, he became Research Scientist in the Macromolecular Physics Department of the Institute for Structure of Matter (CSIC), Madrid. Dr. Ania research interests are mainly devoted to investigate the physical properties of polymer systems in relation to their nanostructure. Since 1990, he has regularly visited several synchrotron radiation sources (DESY, ESRF, BNL) to use X-ray diffraction methods in the investigation of real-time structural changes produced by external fields. He has been involved in studying polymer liquid crystals, high performance polymers, composites, block copolymers and other nanostructural assemblies of polymers. He has published over 60 papers and several book chapters.

Professor Francisco J. Baltá-Calleja, Senior Scientist – Institute for Structure of Matter, CSIC, Madrid. He studied Physics at the University of Madrid and gained a B.Sc. in 1958, after which he obtained a Research fellowship at the University of the Sorbonne in Paris. In 1959 he obtained a Ramsay Memorial Fellowship at the H.H. Wills Physics Laboratory University of Bristol and gained a Ph.D. in 1962. In 1963 he obtained an Alexander von Humboldt Fellowship in the Fritz Haber Institute, Max Planck Society in Berlin. In 1965 he took up a lectureship in Electricity and Magnetism at Madrid University. In 1967 he became Research Associate at the Research Triangle Institute, North Carolina. He became Head of the Macromolecular Physics Department of the Institute for Structure of Matter (CSIC), Madrid in 1975 and Research Professor in 1984. From 1986 till 2003 was the Director of the Institute for Structure of Matter. Prof. Baltá-Calleja also chaired the Solid State Physics Group of the Spanish Royal Society of Physics (1988–1992) and the Macromolecular Physics Board of the European Physical Society (1994–2001). Prof. Baltá-Calleja research interests focus in inter-relating nanostructure, processing and dynamic changes in polymers, by means of X-ray diffraction methods using synchrotron radiation, and physical properties (micromechanical, electrical, magnetic properties, etc.) of advanced polymers, liquid crystalline systems and composites. He published over 380 papers and several books. He has lectured as invited Professor in several Institutions; University of Ulm, University of Hamburg, University of Leeds, University of Shizuoka, Case Western Reserve University, Cleveland. In 1996 he was elected as a Fellow of the Royal Academy of Science of Barcelona and in 2008 Member of the German Academy of Plastics Innovation.